An Elasto-Visco-Plastic Multiscale Model for Fibrous Unidirectional Composite Materials

by

Shari Lynn King

A thesis
presented to the University of Waterloo
in fulfillment of the
thesis requirement for the degree of
Master of Applied Science
in
Mechanical Engineering

Waterloo, Ontario, Canada, 2016

I hereby declare that I am the sole author of this thesis. This is a true copy of the thesis, including any required final revisions, as accepted by my examiners.

I understand that my thesis may be made electronically available to the public.

Abstract

This research thesis investigates the capability of predicting the elasto-visco-plastic material response and failure of a unidirectional composite material. A constitutive framework is developed to incorporate the elastic, plastic and rate sensitive response of composite materials to enhance the simulation capabilities of composite materials for industrial use. Numerical simulations are paramount to facilitating component design at a large scale. In this thesis, a multiscale model is developed from a micromechanics basis in order to predict the macroscopic material behaviour. This model is implemented in an LS-DYNA user-defined material model and incorporates a stress-based failure criteria created for composites. The simulated material response is compared to multiple cases of experimental data from literature, and shows strong agreement with the results. It is recommended that damage and temperature dependence be incorporated into this model in future work.

Acknowledgements

I would like to thank Kaan Inal for his support as my supervisor throughout this project, and for suggesting the topics for my thesis. I would also like to thank Trevor Sabiston for being a mentor in composite materials. Not only did he facilitate useful technical discussions and provide editing assistance, but he also aided in developing the constitutive phenomenological framework on which my work is based. I would like to thank Christopher Kohar for his help in debugging my model and providing code, and I'd like to thank the CMRG research group for providing a place to bounce ideas around. Thanks to my boyfriend, Kornel Niedziela, for helping motivate me through my degree. Lastly, I'd like to thank my parents their editing assistance and for trying to understand my work through the use of bread and pasta analogies.

Table of Contents

List of Tables

List of Figures

Nomenclature

C_f	Constitutive matrix for the fibre
C_m	Constitutive matrix for the matrix
E_{fa}	Axial Young's modulus of the fibre
E_{ft}	Transverse Young's modulus of the fibre
E_m	Young's modulus of the matrix
F	Total deformation gradient
F_m	Deformation gradient in the matrix
G	Displacement gradient
G_f	Shear modulus in the fibre
G_{gf}	Displacement gradient in the fibre
G_m	Shear modulus in the matrix
G_{gm}	Displacement gradient in the matrix
hm	Strain rate exponent
h'	Hardening parameter
I_1	First invariant of a tensor
k	Material pairing constant
K_m	Matrix hardening modulus
l	Material pairing constant
m	Material pairing constant
MTc	Mori-Tanaka parameter
N_m	Matrix hardening exponent
Q	Overall constitutive law
r_{if}	Finish radius of the interphase zone
r_{im}	Radius of the interphase zone
r_{is}	Start radius of the interphase zone
S_c	Shear strength of composite

$\mathbb{T}$	Strain transformation (localization) tensor
V_f	Volume fraction of the fibre
V_{fe}	Effective volume fraction of the fibre
V_{me}	Effective volume fraction of the matrix
X_c	Longitudinal compressive strength of composite
X_t	Longitudinal tensile strength of composite
Y_c	Transverse compressive strength of composite
Y_t	Transverse tensile strength of composite
α	Fitting constant in failure criteria
α_m	Pressure sensitivity of matrix material
δ_{ij}	Kronecker delta
ε	Overall strain
ε_f	Strain in the fibre
ε_m	Strain in the matrix
ε_m^{el}	Elastic strain in the matrix
ε_m^{pl}	Plastic strain in the matrix
$\dot{\varepsilon}$	Strain rate of matrix
$\dot{\varepsilon}_o$	Reference strain rate
ν_{ft}	Transverse Poissons ratio for the fibre
ν_{fta}	Transverse axial Poissons ratio for the fibre
ν_m	Poisson's ratio for the matrix
σ	Overall stress
$\sigma^{'}$	Deviatoric component of stress
σ_f	Stress in the fibre
σ_m	Stress in the matrix
σ_{ym}	Yield stress of the matrix

Chapter 1

Introduction

Since the use of composite materials is becoming more common, industry is looking for inexpensive ways to develop their materials. Composite materials are becoming more attractive due to their inherent ability to have properties tailored for a specific application. In addition, they have the added benefit of being lightweight, and having higher specific strengths and stiffness when compared to metals [9]. However, since there is such a range of variation of properties in composite materials, it is difficult to create a component without extensive testing to know how each combination would perform under a given set of loading conditions.

Rather than spending time and money to manufacture and test a composite, more and more companies are turning to computer-aided modelling to generate some knowledge of material behaviour prior to manufacturing. Use of this approach drastically reduces composite development time and costs. In order for modelling tools to become more prevalent in industrial use, more accurate models need to be developed.

1.1 Research Objectives

This work aims to improve upon the accuracy of existing modelling capability of composite materials. The advances and limitations of existing research are addressed in order to develop a new constitutive framework for modelling failure in a composite material. This new model incorporates micromechanics with phenomenological elasto-visco-plasticity, effectively creating a multi-scale model.

The model is an advancement from several existing models in that it has a small number of inputs, and that it primarily contains physically-based parameters. Elasto-visco-plastic experimental data from literature is used to validate the accuracy of the new multi-scale model in tension, compression and shear for two materials. The rate sensitivity of the model is also examined and compared against literature. A parametric study of some of the micromechanics pairing parameters adds to the understanding of the overall model.

The ultimate end result of this research is that a new phenomenological material model will be generated - one which will be used to model the behaviour in complex part geometries, as well as to determine the mode of failure.

1.2 Thesis Outline

The structure of this thesis is as follows:

Chapter 2 provides the background and motivation for this research. It develops the conventional axis directions for a composite material and the typical failure modes. Throughout this chapter, the relevant literature is discussed relating to unidirectional materials, the development of micromechanics and representative volume elements, and multi-scale models. The importance of plasticity and strain rate effects are considered, and the homogenization scheme is presented. An overview of composite failure and several of the most common failure criteria are presented in order to provide the reader with some background. Last, the existing finite element models which are implemented in the LS-DYNA software are discussed for thoroughness.

In Chapter 3, the constitutive framework for the overall model is put forward. The model first began as a purely elastic model, before developing into an elasto-visco-plastic model. Mathematics pertaining to strain-rates, flow rules, yield criteria, and hardening are presented. In addition, the potential limitations of this model are examined.

The results of this model are presented in Chapter 4. In order for any reader to reproduce the work, the input model parameters are provided for the elastic and the elastic-visco-plastic cases for several different materials. A parametric study is performed to show the effects of the pairing parameters in the elasto-visco-plastic model. Stress-strain curves are given for comparison between the experimental data, existing models and this new model.

Chapter 5 gives a summary of the rest of this thesis. Conclusions as to the usefulness and validity of the model are provided. Future suggestions for extension of this work are given in Chapter 6.

Chapter 2

Background and Motivation

A composite material (or composite, for short) is a material that is made up of two or more constituents. These materials are designed with the aim that the final product has better properties than the individual components for a given application. In general, for structural components, there are two types of composite materials; multiphase and laminated. Multiphase composites contain spherical or cylindrical inclusions within a matrix, and can be randomly distributed or uniformly aligned. Laminated composites consist of multiple layers of multiphase composites which are bonded together.

For a composite material, the conventional material directions are used. The longitudinal or axial direction is along the fibre direction, whereas the transverse direction is at 90° to the fibres. The normal direction is orthogonal to the plane between the axial and the transverse directions. This coordinate frame is illustrated in Figure 2.1.

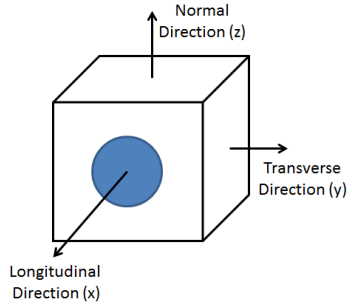

Figure 2.1: Material directions

A composite can fail in several ways, as shown in Figure 2.2. There is fibre breakage or fibre pull-out if tension is applied in the longitudinal direction. If the toughness of the interface (strength of the bond holding fibre and matrix together) between the fibre and matrix is low, then fibre-matrix debonding occurs instead of fibre breakage [40]. In compression of the overall material, the fibres are compressed, creating fibre micro-buckling. In the transverse direction, there is matrix cracking or splitting. Depending on the loading, shear stresses can also split the matrix material. A composite laminate can also fail through delamination, though this failure phenomenon is outside the scope of this thesis.

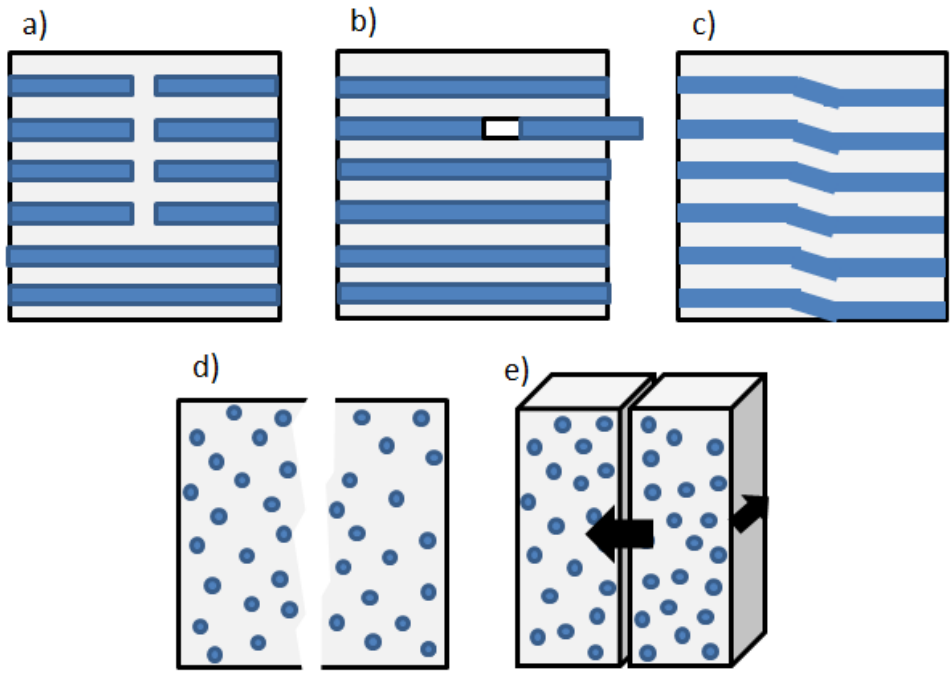

Figure 2.2: Modes of composite material failure through a) fibre breakage b) fibre pull-out c) fibre micro-buckling d) matrix cracking e) shear

2.1 Unidirectional Composites

At a micro scale, if a material is considered non-homogeneous, the stress and strain throughout the composite material differs due to the proximity to inclusions in the material. Es-

helby developed equations that explained the effects of an inclusion on the overall material [22]. As a material is strained, stress tractions are introduced around the inclusion in order to maintain the bond between the inclusion and the surrounding material. Using Eshelby's work, the stress and strain just outside the inclusion is calculated, along with the far-field effects [22, 23]. The relation between the constrained strain and the stress-free strain is given by Eshelby's inclusion tensor, discussed further in Chapter 3. This inclusion tensor changes based on the inclusion shape [22] - be it spherical, ellipsoidal or cylindrical. However, Eshelby's work idealizes the bond between the inclusion and the surrounding material as being perfectly bonded. Qu extended this work by developing a modification to the Eshelby tensor when the bond in the composite is imperfect [65].

To model the mechanics of the overall material, Tsai developed analytical relations between material parameters of the constituents and the overall unidirectional composite material coefficients [79]. Tsai's equations allow constituent material properties to be tailored in order to design a composite to accurately meet a specific overall property. From there, Tsai went on to state that the strength of a unidirectional composite is governed by its strengths in the transverse, axial and shear directions [80]. This work was extended by Adams and Tsai, where they suggested that the fibre packing in a multiphase composite affected the strengths and stiffness [3]. Hsu et al. confirmed this hypothesis by showing a comparison of stress-strain curves for different packing sequences [38]. However, the equations developed by Tsai to predict material properties held regardless of fibre packing sequence.

Hill created a self-consistent method for estimating the elastic modulus based on the work of Eshelby. He reasoned that Eshelby's work is valid if the volume fraction of inclusions is sufficiently small within the matrix material [32]. These findings were important in that they provided a basis for unit cell modelling and representative volume elements. The overall behaviour of a composite material is able to be predicted through the micromechanics work by Aboudi [1]. Through this, the response and failure curves of many types of composites are predicted.

2.2 Micromechanics

By examining a composite material at a small scale, it is clear that there are interactions between the fibre and the matrix components. One key approach is used to extend the behaviour of the material at the microscopic scale to the material as a whole. Representative volume elements (RVE) are used to generalize how the composite acts, and are the smallest element that can be made of any repeating microstructure [63]. In a typical RVE,

there are two main fibre packing methods, as shown in Figure 2.3, where both hexagonal and square packing sequences are shown.

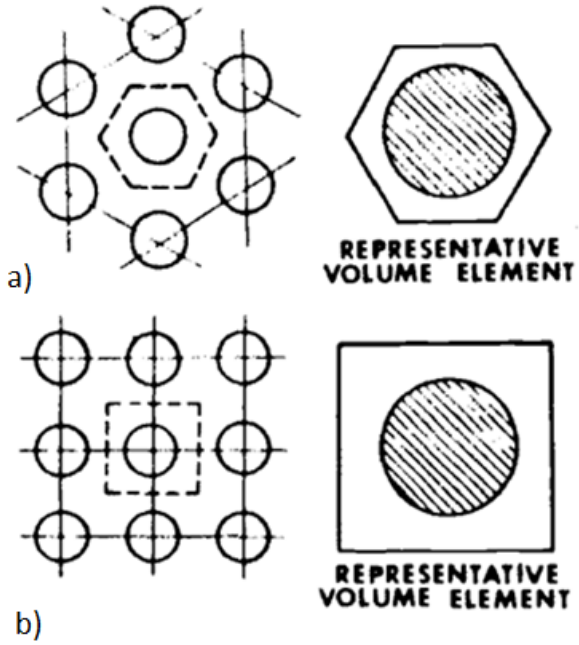

Figure 2.3: Fibre packing methods a) Hexagonal b) Square [5]

The interaction between the fibre and the matrix at a micro scale is shown in different ways. Some models use cohesive zones to model the area between the fibre and the matrix and uses finite element analysis (FEA) software in this region. The fibre and the matrix are meshed individually and the interaction between these two materials is modelled using a layer of cohesive elements. Other methods use constitutive framework to mathematically model the physical interface between the fibre and matrix.

Cohesive zones are used primarily in FEA where a layer of elements surround the fibre where the fibre and matrix have separate properties. Research suggests that modelling the bond between the fibre and the matrix with this zone is important as the strength of the bond influences damage microscopically [58]. Others argue that the effect of the interface between the fibre and the matrix material is negligible [12]. Regardless of the exact impact of this interface, some micromechanics methods do model the zone between the fibre and matrix. However, modelling these cohesive zone elements is computationally

expensive, as the fibres have to be modelled at their correct size using a fine mesh [46]. In addition, contact algorithms which capture interactions between components also add to the computation time.

Another method of modelling the interaction between the fibre and matrix is to generalize their interaction through use of an interphase. An interphase is a region between the fibre and matrix that has its own material properties. The bond between the fibre and matrix is often characterized as being perfect, and continuity is enforced to model this connection [22]. In reality, this isn't the case. There are imperfections in the bond which could be caused by phenomena such as an improper coating of the fibres, or by fibre roughness, and as such, the region between the constituents needs to be modelled by an interphase. The effect of imperfect interfaces was investigated by Benveniste, and Achenbach and Zhu [2, 7].

Work by Sabiston et al. used an interphase approach to model this imperfect interface by using a functionally graded interphase zone [68, 69]. One benefit of using this interface approach is that it is able to address the benefits of both the cohesive zones and the interphase approach. This work took the square representative volume element shown in Figure 2.3 and built upon that model, as detailed in Section 2.2.1.

2.2.1 Sabiston Model

Since much of the work in this thesis is developed based on the work by Sabiston et al. [68, 69], it is advantageous to expand on this model. The Sabiston model takes the concept of a perfectly-bonded unit cell, and extends it, such that the fibre within the cell is a representation of a number of fibres within the material. The radius of this representative fibre is calculated as a function of the fibre volume fraction.

Rather than physically examining the interface between the fibre and matrix, this model uses a numerical functionally-graded interphase zone. The bounds of this zone are constitutively modelled using a function of the distance from the fibre as a function of the fibre radius. The initial model is capable of finding the overall elastic material response based on the constituent properties [69]. From there, the model is extended to find the elasto-visco-plastic response, where strain-rate effects have been incorporated [68].

2.3 Multi-Scale Models

In practice, people wish to use composite materials to build parts for a specific application. It is useful to know the properties of the constituents, but it is more useful to be able to know the properties of the overall material. By having knowledge of the role that the constituent properties play is important in constructing constitutive laws for the composite. This type of multi-scale model is gaining popularity after several decades of strong developments in micromechanics [63]. Hashin developed equations to calculate the effective moduli and Poisson's ratios for an anisotropic composite material regardless of the fibre packing sequence, based on the relation between an isotropic and transversely isotropic phase [29].

2.3.1 Homogenization

Homogenization schemes are used to generalize the response of a heterogeneous material, like a composite, which allows for the approximation of the material response. Mean field theories use the averages of the constituent response within a material to find the overall response [62]. These are rather useful since they use the concept of the RVE rather than physically modelling an RVE, which can be computationally expensive. The mean field methods of homogenization of most relevance are the self-consistent scheme and the Mori-Tanaka scheme. One shortcoming of many micromechanics models is their inability to separate the overall stress into the components acting on the fibre and the matrix [69], but because it is desirable to separate the stresses, homogenization schemes are used.

The Self-Consistent Scheme

The self-consistent scheme is used to calculate the stress or strain tensors in the inclusion (i.e. a fibre) from the macroscopic moduli based on the solution developed by Eshelby [63]. It was adapted for unidirectional composites by Hill through the assumption that the average strain in the inclusion is the strain in all inclusions, which is correct in some cases, but not all [63].

The scheme approximates the effective mechanical properties of the material, but one shortcoming is that it is unable to explicitly take into account the matrix phase. It works based on the premise that each inclusion in an infinite matrix behaves as if there were no other inclusions around. In this way, no other inclusions have any effect on the original inclusion [21]. This body then is operated upon by a remote strain, and the strain in the inclusion is found.

The Mori-Tanaka Scheme

The Mori-Tanaka approach to homogenization calculates the average stress in the matrix from the Eshelby solution and was proposed by Mori and Tanaka [54]. The average strain in the fibre is related to the strain in the matrix through a strain concentration matrix [63], which is given as $\mathbb{T}$ in this thesis.

Unlike the self-consistent scheme, the average contributions of the matrix phase are taken into account, which can lead to an over-estimation of the material response in some loading cases. A shortcoming of the Mori-Tanaka scheme is that the symmetry of the stiffness matrix can be lost under certain loads [63].

The method in which this scheme calculates the stiffness matrices allows for a great deal of variation in terms of the shape of inclusion in the composite. Much like in the self-consistent scheme, the inclusion behaves as if it were alone in an infinite matrix. However, in this scheme, the body is acted upon by an average matrix strain, at which point the strain in the inclusion can again be found [21].

2.3.2 Plasticity

It is known that the fibre materials, such as carbon fibre or glass fibre, behave in an elastic manner. They are capable of stretching until they reach their failure strength and break, all within the elastic regime. The surrounding polymer matrix material, such as epoxy, is known to behave elasto-visco-plastically, so both plasticity and rate-dependency must be taken into account in the constitutive models.

In the axial direction, the composite material behaviour is dominated primarily by the elastic response of the fibres. The transverse and shear stress-strain curves are dominated by the matrix material response [11, 37, 47]. However, composites do have a limited ability to undergo plastic deformation before failure [9]. The plastic formulation for this model is given in Section 3.2.

Hill extended the Von Mises model for the orthotropic case in metals, though this still had limitations when it came to materials that used J2 terms [10, 33]. Anisotropic yield functions were proposed by authors such as Budiansky and Barlat [10]. From this point, plastic models which were specifically developed for composite materials were required.

Sun and Chen developed two simple plane stress models for orthotropic plasticity in unidirectional composites based on Hill's plasticity theory, as well as a three-dimensional orthotropic model [15, 74, 75]. The first model capitalizes on the elasticity of the fibres and

uses one parameter to describe plasticity, but only in the transverse direction [74]. The second model uses J2 flow theory to model the elasto-plasticity of a metal-matrix material through a rudimentary quarter-symmetry RVE [75].

The three-dimensional Chen and Sun model assumes anisotropic composite properties. As with the previous Sun and Chen models, J2 flow theory is used, and an RVE model is developed with a coarse mesh to model the elasto-plastic behaviour of the composite [15], because using a coarse mesh reduces numerical computational time. However, most input fitting parameters in this models have no physical basis, though one parameter in the last model is based on elastic properties.

Xie and Adams created a three-dimensional plastic FEA model for testing stress distributions [85]. A plastic associative flow rule is used along with a quadratic yield function in order to develop the plastic stress-strain relationship. This model provides good results, but uses multiple fitting parameters which have no apparent physical basis and are determined through trial and error [85].

2.3.3 Strain Rate

The response of a composite material varies with changing strain rate, as fracture strain is shown to decrease with increasing strain rate, as shown by Reis et al. [66]. In tension, whether the strain rate has an effect on material behaviour is still under discussion. Several studies have shown that strain rate has an effect [20, 31, 57, 59, 78], but an overall consensus is not clear due to studies to the contrary [19, 60, 61, 72].

However, in compression, strain rate is shown to play a strong role, as an epoxy-type matrix material has strong rate effects [48, 57]. Some fibres, like carbon, are not rate sensitive, but glass fibres do show rate dependency [9, 26]. Stress/strain plots by Lindholm show that the epoxy material behaves elasto-visco-plastically as recovery is observed [48, 82]. The matrix material hardens as strain increases, which provides support for the fibres. Research done by Yuan et al. shows that compressive strength increases as strain rate increases in composites with glass fibres [86].

A constitutive model of this rate-dependent behaviour by Karim and Hoo Fatt uses stress relaxation equations for the matrix material [43]. Little other research has been conducted into developing constitutive equations with rate-dependency for composite materials due to difficulties in dealing with an anisotropic material [43]. In addition, there is still difficulty with higher strain rate testing to get material data [37]. Instead of relaxing equations, two different scaling rules are applied to the effective stress/plastic strain curve in the works by Weeks and Sun, and Kallimanis and Kontou [42, 84].

2.4 Failure

In addition to knowing how a unidirectional composite behaves, it is pertinent to know when the material fails, since most fail in a brittle way. For glass fibre reinforced composites, failure is ductile at low volume fractions (<30-40%), but brittle at higher volume fractions [86]. Failure occurs when a material is no longer able to perform its function [34], and often occurs suddenly [41]. Multiple failure criteria have been developed for composite materials, but there is still a lack of confidence in being able to accurately predict failure in a given material for any loading path. Most failure criteria tend to be conservative [34].

There are a few overarching theories which model failure and damage. Continuum Damage Mechanics (CDM) analyzes damage, fracture and failure of a material from the point of view of continuum mechanics, as the name suggests [56]. The aim of CDM is to model the initiation and progression of damages to a material at the macroscopic or mesoscopic levels. As important as it is to know how damage progresses through a material, this problem is outside the scope of this thesis.

Classical Lamination Theory (CLT) is used to model the behaviour of stacks of unidirectional composite layers. The biggest mode of failure for laminates is through delamination, and CLT is able to aid in the prediction of first ply failure and in buckling[70, 73]. Since this thesis focuses on a unidirectional material, laminated material failure is outside the scope.

Azzi and Tsai began much of the work on composite failure theories based on Hill's work for anisotropic metals [4]. This was one of the first works which began referring to the yield stress of composite materials as the strengths in a respective direction [76]. Hoffman implied that failure in a composite was brittle [35], though this isn't the case for all materials in all failure modes. The benefit of this work is that Hoffman began assigning different strengths for different directions in materials, though he acknowledged that a limitation of his work was its inability to predict the mode of failure [35, 76].

Tsai and Wu continued the initial work of Hoffman for creating scalar functions to describe an ellipsoidal failure surface in terms of the strength parameters [81], the equations for which are given in Section 2.4.1. Since there are multiple ways to calculate the shear strength, Hashin noted that the Tsai-Wu failure criteria produced a failure surface which was not applicable in all cases [76]. He suggested that a piecewise smooth failure surface be used instead of the ellipsoidal surface [30]. Hashin also separated failure into the individual failure modes. At this point, it was clear that failure in composite mechanics needed to be based on the mechanisms of how the materials failed.

As part of the World Wide Failure Exercise spanning from 1998 through to 2004, Hinton and Soden generated a comprehensive analysis of several emerging failure theories for fibre-reinforced composite materials [73]. As mentioned before, having a method of discerning between modes of failure is a useful characteristic to have in a model, as it allows the designer to more accurately predict the material behaviour. Of the theories examined in this failure exercise, the theories by Chamis, Edge, Hart-Smith, McCartney, Puck, Rotem, Sun, Tsai, Wolfe, and Zinoviev are able to differentiate between failure modes [73].

Several theories also use micromechanics-based formulations [73]. The theory by Chamis uses the constituent properties to predict the properties of each lamina [24]. The Hart-Smith theory develops failure strain limits from the fibre and matrix properties [27, 28]. After failure is initiated, Tsai's theory uses micromechanics to predict the development of the failure [49]. To calculate the failure criterion for the matrix material, the theory by Rotem requires the matrix properties [67]. Puck's theory uses fibre properties to generate failure envelopes [64]. However, these theories use micromechanics for failure prediction rather than as part of constitutive laws for the overall material. In addition, correctly predicting failure of a material based on micromechanics requires the ability to predict micro-failure in the material, which is often challenging [30].

Alternatively, failure of a composite material can be predicted based on the average stress or strain in the overall material on a macroscale level. Hashin introduced failure criterion based on this [30]. Much of Hashin's work was extended by Yamada and Sun, which was later extended into the Chang and Chang criteria.

In many composite laminates, failure does not occur at the point when the first failure is detected in a ply. Due to the laminate stacking sequence, a ply may fail in one direction, while the surrounding plies may still be able to carry the load. At this point, the overall strength of the material is reduced, but the overall material has not failed. To model this phenomenon, material properties are degraded to simulate the weakening of the material overall, such as seen in the work by Barbero et al., Lopes et al., Moure et al., Maimi et al., Liu and Zheng, and Cheng and Binienda [6, 16, 50, 51, 53, 55].

2.4.1 Failure Criteria

Some of the more prominent failure criteria are mentioned in order to highlight equations.

Maximum Stress Criterion

In the maximum stress theory (also called the Rankine criterion), failure occurs if stress in any direction is greater than the corresponding strength in that direction. This is illustrated by the conditions shown in Eqs. 2.1, 2.2 or 2.3. This criterion is adequate for brittle materials, since they fail by fracture, but is inadequate for ductile materials [8, 44]. F_{1t} and F_{1c} are the longitudinal strength in tension and compression, and F_{2t} and F_{2c} are the transverse strength in tension and compression, respectively. F_{12} is the strength in shear. σ_1, σ_2 and σ_{12} are the stresses in the longitudinal, transverse and shear directions.

$$\sigma_1 < F_{1t} \qquad or \qquad |\sigma_1| < F_{1c} \tag{2.1}$$

$$\sigma_2 < F_{2t} \qquad or \qquad |\sigma_2| < F_{2c} \tag{2.2}$$

$$|\sigma_{12}| < F_{12} \tag{2.3}$$

Maximum Strain Criterion

Maximum strain theory (or St. Venant's criterion) is similar to the maximum stress theory shown above. Failure occurs if the strains along each axis are greater than the allowable strain, shown by Eqs. 2.4, 2.5 or 2.6 [8, 44]. ε^u_{1t} and ε^u_{1c} are the longitudinal ultimate strain in tension and compression, and ε^u_{2t} and ε^u_{2c} are the transverse ultimate strain in tension and compression, respectively. γ^u_{12} is the ultimate strain in shear. ε_1, ε_2 and γ_{12} are the strains in the longitudinal, transverse and shear directions.

$$\varepsilon_1 < \varepsilon^u_{1t} \qquad or \qquad |\varepsilon_1| < \varepsilon^u_{1c} \tag{2.4}$$

$$\varepsilon_2 < \varepsilon^u_{2t} \qquad or \qquad |\varepsilon_2| < \varepsilon^u_{2c} \tag{2.5}$$

$$|\gamma_{12}| < \gamma^u_{12} \tag{2.6}$$

Tsai-Hill Criterion

The Tsai-Hill theory was based on the distortion energy failure theory from the Von Mises yield criterion, which was then developed for composite materials by Azzi and Tsai [4, 44]. Failure is said to occur in this theory if Eq. 2.7 is greater than one. The terms in the Tsai-Hill criterion are the same as in the Maximum Stress criterion.

$$\left(\frac{\sigma_1}{F_{1t}}\right)^2 - \left(\frac{\sigma_1}{F_{1t}}\right)\left(\frac{\sigma_2}{F_{1t}}\right) + \left(\frac{\sigma_2}{F_{2t}}\right)^2 + \left(\frac{\sigma_{12}}{F_{12}}\right)^2 < 1 \tag{2.7}$$

It is clear that this equation mostly has tensile strengths in it. As such, the following modifications should be made depending on the load case. If σ_1 <1 then F_{1t} should be replaced with F_{1c} in the first two terms, and if σ_2 <1 then F_{1t} should be replaced with F_{1c} in the second portion of the second term. If σ_2 <1 then F_{2t} should be replaced with F_{2c} in the third term.

Tsai-Wu Criterion

For anisotropic materials, the general Tsai-Wu failure criterion is defined as seen in Eq. 2.8, where F_i and F_{ij} are second and fourth order strength tensors [81]. This was derived from the total strain energy failure theory by Beltrami [44]. The Tsai-Wu criterion improves upon the Tsai-Hill criterion, as it is able to differentiate between the tensile and compressive strengths.

$$F_i\sigma_i + F_{ij}\sigma_i\sigma_j < 1 \tag{2.8}$$

For a plane stress condition, Eq. 2.8 can be written as in Eq. 2.9.

$$F_1\sigma_1 + F_2\sigma_2 + F_{11}\sigma_1^2 + F_{22}\sigma_2^2 + F_{66}\tau_{12}^2 + 2F_{12}\sigma_1\sigma_2 < 1 \tag{2.9}$$

The coefficients are given as in Eqs. 2.10, 2.11 and 2.12, where i varies between 1 and 3, and where N_i^+ and N_i^- are the tensile and compressive strengths, and S_6 is the shear strength.

$$F_{ii} = \frac{1}{N_i^+ N_i^-} \tag{2.10}$$

$$F_i = \frac{1}{N_i^+} - \frac{1}{N_i^-} \tag{2.11}$$

$$F_{66} = \frac{1}{S_6^2} \tag{2.12}$$

Hashin Criterion

Quadratic failure criterion were developed by Hashin to distinguish between failure modes for a composite lamina based on the stresses in the overall material [30], since the above theories do not take the failure mode into account. The fibre and matrix each have two modes of failure, tension and compression. For the fibre, the tension and compression failure criteria are given in Eqs. 2.13 and 2.14. σ_A^+ is the tensile failure stress in the fibre direction, and σ_A^- is the compressive failure stress in the fibre direction. Similarly, σ_T^+ and σ_T^- are the transverse failure stresses in tension and compression, respectively. τ_A and τ_T are the axial and transverse failure shear stresses.

$$\left(\frac{\sigma_{11}}{\sigma_A^+}\right)^2 + \frac{1}{\tau_A^2}(\sigma_{12}^2 + \sigma_{13}^2) = 1 \tag{2.13}$$

$$\sigma_{11} = -\sigma_A^- \tag{2.14}$$

For the matrix material, the tension and compression failure criteria are given in Eqs. 2.15 and 2.16, respectively.

$$\frac{1}{\sigma_T^{+2}}(\sigma_{22} + \sigma_{33})^2 + \frac{1}{\tau_T^2}(\sigma_{23}^2 + \sigma_{22}\sigma_{33}) + \frac{1}{\tau_A^2}(\sigma_{12}^2 + \sigma_{13}^2) = 1 \tag{2.15}$$

$$\frac{1}{\sigma_T^-}\left[\left(\frac{\sigma_T^-}{2\tau_T}\right)^2 - 1\right](\sigma_{22}+\sigma_{33}) + \frac{1}{4\tau_T^2}(\sigma_{22}+\sigma_{33})^2 + \frac{1}{\tau_T^2}(\sigma_{23}^2+\sigma_{22}\sigma_{33}) + \frac{1}{\tau_A^2}(\sigma_{12}^2+\sigma_{13}^2) = 1 \tag{2.16}$$

Chang and Chang Failure Criterion

The Chang and Chang failure criterion is an extension of the Yamada Sun model, which itself is based on the Hashin-Rotem criterion [13, 14]. This model is capable of predicting failure in three modes: matrix failure, fibre failure, and compression. After failure, the mechanical properties are reduced based on a property degradation model.

Matrix failure (Eq. 2.17) occurs if $e_m \geq 1$, where σ_{22} is the stress in the transverse direction, Y_t is the tensile strength in the transverse direction, and G_{12} is the shear stress. S_c is the shear strength, and α is a fitting parameter defined from shear stress-strain

measurements [25]. If matrix failure occurs, then the constitutive properties E_{ft}, G_f, ν_{ft} and ν_{fta} are reduced to zero [25].

$$\left(\frac{\sigma_{22}}{Y_t}\right)^2 + \frac{\frac{(\sigma_{12})^2}{2G_{12}} + \frac{3}{4}\alpha(\sigma_{12})^4}{\frac{(S_c)^2}{2G_{12}} + \frac{3}{4}\alpha(S_c)^4} = e_m^2 \tag{2.17}$$

Fibre failure occurs if $e_f \geq 1$, where σ_{11} is the stress in the axial direction and X_t is the tensile strength in the axial direction (Eq. 2.18). If fibre failure occurs, then E_{fa}, E_{ft}, G_f, ν_{ft} and ν_{fta} are reduced to zero [25].

$$\left(\frac{\sigma_{11}}{X_t}\right)^2 + \frac{\frac{(\sigma_{12})^2}{2G_{12}} + \frac{3}{4}\alpha(\sigma_{12})^4}{\frac{(S_c)^2}{2G_{12}} + \frac{3}{4}\alpha(S_c)^4} = e_f^2 \tag{2.18}$$

Compressive failure occurs if $e_c \geq 1$, where Y_c is the compressive strength in the transverse direction, as in Eq. 2.19. If compressive failure occurs, then E_{ft}, ν_{ft} and ν_{fta} are reduced to zero [25].

$$\left(\frac{\sigma_{22}}{2S_c}\right)^2 + \left[\left(\frac{Y_c}{2S_c}\right)^2 - 1\right]\frac{\sigma_{22}}{Y_c} + \frac{\frac{(\sigma_{12})^2}{2G_{12}} + \frac{3}{4}\alpha(\sigma_{12})^4}{\frac{(S_c)^2}{2G_{12}} + \frac{3}{4}\alpha(S_c)^4} = e_c^2 \tag{2.19}$$

2.5 Current LS-DYNA Composite Material Models

The constitutive equations of Chapter 3 need to be solved through a numerical solver. LS-DYNA is a simulation software which is used to run a finite element analysis. This software has multiple built-in material models, as well as the capability to run user defined material models (UMAT). This model has been implemented into one of these UMATs.

LS-DYNA contains seven composite models in the general license, but most are intended for use with laminated materials. MAT_022 is a composite damage model for orthotropic materials [52]. This model has the option for brittle failure and laminate theory, and uses the Chang and Chang failure criterion [13, 14]. MAT_022 is extended in MAT_054 and MAT_055 for thin shell elements, where the MAT_055 model uses the Tsai-Wu failure criterion [52, 81]. MAT_054 allows the user to model anisotropic, linear elastic material for any initially undamaged material. From that point, nonlinearity is introduced by degradation of material properties through the damage criteria [71].

MAT_058 is a laminated composite fabric model intended for plane stress conditions, with additional strain rate effects incorporated into MAT_158 [52]. The elastic parameters in MAT_058 are modified using a damage model which assumes microcracks and cavities develop due to deformation [71]. An elasto-plastic composite failure model was provided in MAT_059 [52]. Both models MAT_054 and MAT_059 have the capability to perform element erosion upon failure [71].

The composite layup material model, MAT_116, is useful for modelling a composite with an arbitrary number of layers, without using laminate shell theory [52]. This is useful if a large number of layers are to be run. MAT_117 and MAT_118 are used for modelling the elastic response of a uniform thickness composite where rather than material properties, the stiffness coefficients are provided for the material and element coordinate systems [52].

In addition to the aforementioned models, there are a few proprietary models requiring additional licensing. MAT_161 can be used to model progressive failure for unidirectional and woven fabrics based off work by Hashin [30, 52]. MAT_162 is an extension on the previous model which allows a damage mechanics approach for softening behaviour [52]. A sub-laminate-based continuum damage model, MAT_219 was also developed for fibre reinforced composite laminates, where the stiffness matrix is reduced based off reduction coefficients [52].

It is seen that the existing models are useful for modelling a laminated material, but may have difficulty incorporating the entire elasto-visco-plastic behaviour that is known to occur in composite materials. In addition, many of these models are used with shell elements, and cannot be run with solid brick elements. Currently, there does not appear to be a readily available model for modelling these unidirectional materials with solid elements, which would allow for three-dimensional information.

2.6 Motivation

For several decades, work has been conducted to improve composite models, both in terms of mechanical behaviour and in failure prediction. Micromechanics models based on representative volume elements provide sound information about the underlying microscopic behaviour of the material. These models continue to get more accurate over time, but need improvement in predicting the overall composite material behaviour on their own. Homogenization schemes have been developed in order to generalize composite behaviour based off the micromechanics models.

There is currently a need to develop a model that is capable of tying together the micromechanics based models with the phenomenological plasticity constitutive laws through an efficient and applicable homogenization scheme. This model should have input parameters that are primarily physically based, which would be directly available from testing or through calculation, in order to improve upon some of the existing models. It should also be based on the interphase approach to modelling the interaction between the fibre and the matrix, as it is less expensive computationally to use the interphase zone approach opposed to using cohesive zone elements.

The new model should also have the capability to capture the rate dependence of the composite behaviour, as loading in a practical application would likely be done using multiple rates. Lastly, this model should incorporate composite failure because knowing the way the composite material fails allows material designers to tailor the properties to provide the best material for an application.

Industry has need of a model such as the one described. The aim of this research work is to provide companies with this model to allow for better predictive capabilities.

Chapter 3

Model Development

This multi-scale model has been developed for unidirectional long-fibre composite materials. Microscale constitutive laws have been developed to model the interaction between the fibre and matrix. These laws are then homogenized over the bulk material to create a phenomenological model.

The micromechanics approach uses a functionally graded interphase zone to model the stress transfer between the fibre and the matrix, and how the fibre and matrix interact. By modelling this interaction mathematically, a representative volume element is used which contains one fibre and the matrix material. Compared to a cohesive zone approach, this approach is more efficient to solve numerically.

Both plasticity and rate-dependency are added to the basic elastic constitutive framework to produce a comprehensive model. Physically-based parameters are used as input, which allows the user to more fully understand the model.

In the following section, the framework for the elastic constitutive laws is developed. Section 3.2 extends the elastic formulation to include a flow rule, hardening, and strain rate sensitivity. Homogenization is performed using the Mori-Tanaka approach in Section 3.3 and the Chang and Chang failure criteria are implemented in Section 3.4.

3.1 Elastic Constitutive Formulation

The strain in the fibre is found by partitioning the overall strain with a fourth-order strain transformation tensor, $\mathbb{T}$, (containing Eshelby's solution for long-fibres), as shown in Eq.

3.1 [69], such that ε_f is the strain in the fibre and ε is the total strain applied to the unit cell.

$$\varepsilon_f = \mathbb{T}\varepsilon \tag{3.1}$$

Stress and strain in the fibre are related through an elastic constitutive law as shown in Eq. 3.2, where σ_f is the stress in the fibre and C_f is the transversely isotropic constitutive law for the fibre [45].

$$\sigma_f = C_f\varepsilon_f \tag{3.2}$$

At this point, Eq. 3.1 can be substituted into Eq. 3.2 to produce Eq. 3.3.

$$\sigma_f = C_f\mathbb{T}\varepsilon \tag{3.3}$$

3.1.1 Strain Partitioning

Through strain partitioning, it is known that the total strain is related to the effective volume fraction of the fibres (V_{fe}) and the matrix (V_{me}), as shown in Eq. 3.4.

$$G = G_{gf}V_{fe} + G_{gm}V_{me} \tag{3.4}$$

The fibre displacement gradient, G_{gf}, is approximately taken to be ε_f due to the small strain assumption in the fibre before failure, as in Eq. 3.5.

$$G_{gf} = \varepsilon_f \tag{3.5}$$

Performing substitution of Eq. 3.1 into Eq. 3.4 gives Eq. 3.6.

$$G = \mathbb{T}\varepsilon V_{fe} + G_{gm}V_{me} \tag{3.6}$$

Rearranging, an equation for the displacement gradient of the matrix (G_{gm}) as a function of strain can be derived. G_{gm} can be approximately taken to be the matrix strain, ε_m, assuming small elastic deformation, as seen in Eq. 3.7

$$\frac{G(1 - \mathbb{T}V_{fe})}{V_{me}} = G_{gm} \tag{3.7}$$

The total displacement gradient, G, is related to the total deformation gradient through the identity tensor, I, (Eq. 3.8).

$$G = F - I \tag{3.8}$$

Therefore, it follows that Eq. 3.8 can be rewritten for the matrix material as Eq. 3.9.

$$F_m = G_{gm} + I \tag{3.9}$$

The strain in the matrix material is then given through Green's strain equation as in Eq. 3.10.

$$\varepsilon_m = \frac{1}{2}(F_m^T F_m - I) \tag{3.10}$$

3.1.2 Stress

For this elastic formulation, it is assumed that the matrix material behaves as an elastic material, which has been shown in the previous chapter to be an inaccurate assumption. This will be developed into an elasto-visco-plastic formulation in Section 3.2. Eq. 3.11 illustrates the stress-strain relation for the matrix.

$$\sigma_m = C_m \varepsilon_m \tag{3.11}$$

Eq. 3.7 can be substituted into Eq. 3.11, which gives Eq. 3.12

$$\sigma_m = C_m \varepsilon \left(\frac{1}{V_{me}} - \mathbb{T} \frac{V_{fe}}{V_{me}} \right) \tag{3.12}$$

It can be seen that the overall stress, σ, is related to the stress of both constituents as seen in Eq. 3.13

$$\sigma = \sigma_m V_{me} + \sigma_f V_{fe} \tag{3.13}$$

where V_{me} can be given as in Eq. 3.14.

$$V_{me} = 1 - V_{fe} \tag{3.14}$$

Substituting ε_m and ε_f into Eq. 3.13 gives Eq. 3.15

$$\sigma = C_m \varepsilon (1 - \mathbb{T} V_{fe}) + C_f \varepsilon \mathbb{T} V_{fe} \tag{3.15}$$

Factoring Eq. 3.15 gives a stress-strain constitutive relation (Eq. 3.16).

$$\sigma = [C_m (1 - \mathbb{T} V_{fe}) + C_f \mathbb{T} V_{fe}] \varepsilon \tag{3.16}$$

Simply, Eq. 3.16 can be rewritten as Eq. 3.17

$$\sigma = Q\varepsilon \tag{3.17}$$

where

$$Q = C_m(1 - \mathbb{T}V_{fe}) + C_f\mathbb{T}V_{fe} \tag{3.18}$$

3.1.3 Determining Constitutive Components

In order to use this stress-strain relation, the components of Q need to be developed. The effective fibre volume fraction is given as seen in Eq. 3.19 and was developed by Sabiston [69].

$$V_{fe} = \frac{\pi}{4}(r_{im})^2 \tag{3.19}$$

The representative interface radius of the interphase zone, r_{im}, is given as shown in Eq. 3.20, where m is a material pairing constant which is bounded between 0 and 1 [69].

$$r_{im} = \frac{1}{30}\sqrt{480m((r_{if})^2 - (r_{is})^2) + 30(r_{if})^2 + 360r_{if}r_{is} + 510(r_{is})^2} \tag{3.20}$$

From there, r_{if} and r_{is} are given as Eq. 3.21, where V_f is the fibre volume fraction, and k and l are other material pairing constants [69]. These pairing constants describe the inner and outer radii of a functionally graded interphase zone between the fibre and matrix material.

$$r_{is} = k\sqrt{\frac{4V_f}{\pi}} \qquad\qquad r_{if} = l\sqrt{\frac{4V_f}{\pi}} \tag{3.21}$$

As such, k is bounded between 0 and 1, and l is bounded as seen in Eq. 3.22.

$$1 < l < \sqrt{\frac{\pi}{4V_f}} \tag{3.22}$$

After substituting Eq. 3.21 into Eq. 3.20, V_{fe} can be shown as in Eq. 3.23.

$$V_{fe} = \frac{\pi}{3600}\left[480m\left(l^2\frac{4V_f}{\pi} - k^2\frac{4V_f}{\pi}\right) + 30l^2\frac{4V_f}{\pi} + 360kl\frac{4V_f}{\pi} + 510k^2\frac{4V_f}{\pi}\right] \tag{3.23}$$

Condensing and simplifying provides Eq. 3.24.

$$V_{fe} = \frac{V_f}{900}\left[480m\left(l^2 - k^2\right) + 30l^2 + 360kl + 510k^2\right] \tag{3.24}$$

Constitutive Matrices

Since the matrix material is elastic and isotropic, the C_m matrix is given as shown in Eq. 3.25, where E_m is the Young's modulus for the matrix material, and ν_m is the Poisson's ratio for the matrix material.

$$C_m = \frac{E_m}{(1+\nu_m)(1-2\nu_m)} \begin{bmatrix} 1-\nu_m & \nu_m & \nu_m & 0 & 0 & 0 \\ \nu_m & 1-\nu_m & \nu_m & 0 & 0 & 0 \\ \nu_m & \nu_m & 1-\nu_m & 0 & 0 & 0 \\ 0 & 0 & 0 & \frac{1-2\nu_m}{2} & 0 & 0 \\ 0 & 0 & 0 & 0 & \frac{1-2\nu_m}{2} & 0 \\ 0 & 0 & 0 & 0 & 0 & \frac{1-2\nu_m}{2} \end{bmatrix} \tag{3.25}$$

The constitutive matrix for the fibre material, C_f, is transversely isotropic, and is given in Eq. 3.26.

$$C_f = \begin{bmatrix} C_{11} & C_{12} & C_{12} & 0 & 0 & 0 \\ C_{12} & C_{22} & C_{23} & 0 & 0 & 0 \\ C_{12} & C_{23} & C_{22} & 0 & 0 & 0 \\ 0 & 0 & 0 & C_{44} & 0 & 0 \\ 0 & 0 & 0 & 0 & C_{44} & 0 \\ 0 & 0 & 0 & 0 & 0 & C_{66} \end{bmatrix} \tag{3.26}$$

where the components of C_f are given as

$$\begin{aligned} C_{11} &= \frac{E_{fa}(1-\nu_{ft})}{\left(1-\nu_{ft}-2\left(\frac{E_{ft}}{E_{fa}}\right)\nu_{fta}^2\right)} \\ C_{12} &= \frac{E_{ft}\nu_{fta}}{\left(1-\nu_{ft}-2\left(\frac{E_{ft}}{E_{fa}}\right)\nu_{fta}^2\right)} \\ C_{22} &= \frac{E_{ft}\left(1-\left(\frac{E_{ft}}{E_{fa}}\right)\nu_{fta}^2\right)}{\left(1-\nu_{ft}-2\left(\frac{E_{ft}}{E_{fa}}\right)\nu_{fta}^2\right)\left(1+\nu_{ft}\right)} \\ C_{23} &= \frac{E_{ft}\left(\nu_{ft}+\left(\frac{E_{ft}}{E_{fa}}\right)\nu_{fta}^2\right)}{\left(1-\nu_{ft}-2\left(\frac{E_{ft}}{E_{fa}}\right)\nu_{fta}^2\right)\left(1+\nu_{ft}\right)} \\ C_{44} &= G_f \\ C_{66} &= \frac{E_{ft}}{2(1+\nu_{ft})} \end{aligned}$$

and E_{fa} and E_{ft} are the axial and transverse Young's modulus for the fibre, ν_{fta} and ν_{ft} are the transverse axial and transverse Poisson's ratios for the fibre, and G_f is the shear modulus.

In elasticity, the strain transformation tensor is a constant matrix dependant on the separate material parameters as mentioned above. This matrix is given in Eq. 3.27.

$$\mathbb{T}= \begin{bmatrix} t_{1111} & 0 & 0 & 0 & 0 & 0 \\ t_{2211} & t_{2222} & t_{2233} & 0 & 0 & 0 \\ t_{2211} & t_{2233} & t_{2222} & 0 & 0 & 0 \\ 0 & 0 & 0 & t_{1212} & 0 & 0 \\ 0 & 0 & 0 & 0 & t_{1212} & 0 \\ 0 & 0 & 0 & 0 & 0 & t_{2323} \end{bmatrix}^{-1} \tag{3.27}$$

where the six parameters in the transformation tensor are

$$t_{1111} = 1$$

$$t_{2211} = \frac{-E_{ft}\nu_m\nu_{fta}(2E_m\nu_{fta} - E_{fa}) - E_{fa}\nu_m(-2E_{ft}\nu_m\nu_{fta} + E_m\nu_{ft} - E_m) - E_{fa}E_{ft}\nu_{fta}}{E_m[2E_{ft}\nu_{fta}^2(2\nu_m - 1) + (\nu_{ft} - 1)(2E_{fa}\nu_m - E_{fa})] - E_{fa}E_{ft}(2\nu_m^2 + \nu_m - 1)}$$

$$t_{2222} = \frac{-\left[(\nu_m - 1)E_m\left(2E_mE_{ft}(2\nu_m\nu_{ft}(2\nu_{fta}^2 + 3\nu_{ft}) - 3\nu_{fta}^2(\nu_{ft} - 1))\right.\right.}{R}$$
$$\frac{\left.\left.+E_{ft}E_{fa}(-\nu_m\nu_{ft} - 3\nu_m - \nu_{ft} + 5) + 2E_{ft}^2\nu_{fta}^2(\nu_m^2 - 1) + E_{fa}E_m(-3\nu_{ft}^2 - 4\nu_m + 3)\right)\right]}{R}$$

$$t_{2233} = \frac{(\nu_m - 1)E_m\left[(\nu_m + 1)\left(2\nu_{fta}^2E_mE_{ft}(4\nu_m - 1) - E_{fa}E_{ft}(8\nu_m\nu_{ft} - 5\nu_{ft} + 1)\right.\right.}{S}$$
$$\frac{\left.\left.-2E_{ft}^2\nu_{fta}^2(4\nu_m - 3)\right) + E_mE_{fa}(4\nu_m - 1)(\nu_{ft}^2 - 1)\right]}{S}$$

$$t_{1212} = \frac{4E_m}{2G_f\nu_m + 3E_m + 2G_f}$$

$$t_{2323} = \frac{8(\nu_m - 1)E_m(1 + \nu_{ft})}{4E_m\nu_m\nu_{ft} + 4E_{ft}\nu_m^2 + 4E_m\nu_m - 5E_m\nu_{ft} + E_{ft}\nu_m - 5E_m - 3E_{ft}}$$

where

$$R = 2E_{fa}E_mE_{ft}(\nu_m(-4\nu_m^2\nu_{ft} + 4\nu_m^2 - 2\nu_m + 3\nu_{ft} - 4) - 2(\nu_{ft} + 1)) \\ + 2\nu_{fta}^2E_m^2E_{ft}(2\nu_m\nu_{ft} + 2\nu_m - 2\nu_{ft} - 1) \\ + (2\nu_m - 1)\Big((\nu_m + 1)\Big(- 8\nu_{fta}^2E_mE_{ft}^2(\nu_m - 3) + E_{fa}E_{ft}^2(4\nu_m - 3)\Big) \\ + E_{fa}E_m^2(\nu_{ft}^2 - 1)\Big)$$

and

$$S = 2E_{fa}E_mE_{ft}(2\nu_m - 1)(\nu_m + 1)\big[2(\nu_m - 1) - \nu_{ft}(2\nu_m - 1)\big] + 4E_mE_{ft}\nu_m\nu_{fta}^2 \\ + (4\nu_m - 3)(2\nu_m - 1)(\nu_m + 1)\big[- 2\nu_{fta}^2E_mE_{ft}^2 + E_{fa}E_{ft}^2(\nu_m + 1)\big] \\ + 2\nu_{fta}^2E_m^2E_{ft}\big[(2\nu_m - 1)\nu_{ft} - 1\big] + E_{fa}E_m^2(\nu_m - 1)(\nu_{ft} - 1)(\nu_{ft} + 1)$$

3.2 Elasto-Visco-Plastic Constitutive Formulation

In general, it is known that fibres primarily behave elastically. However, the matrix material behaves elasto-visco-plastically, which means that it also exhibits rate-dependent plastic behaviour. In order to take this into account, visco-plasticity is incorporated into the constitutive laws. The strain rate for the matrix material, $\dot{\varepsilon}_m$, is now given as in Eq. 3.28, as it is important to be able to determine the strain in the fibre and the matrix in order to correctly implement plasticity. $\dot{\varepsilon}_m^{el}$ and $\dot{\varepsilon}_m^{pl}$ are the elastic and plastic portions of the strain-rate for the matrix material.

$$\dot{\varepsilon}_m = \dot{\varepsilon}_m^{el} + \dot{\varepsilon}_m^{pl} \tag{3.28}$$

The constitutive matrix for the matrix material is modified through a plastic corrector term, $\dot{\lambda}$, given in Eq. 3.29. C_m is the elastic constitutive law for the matrix material (Eq. 3.25), $\frac{\delta F}{\delta \sigma}$ is the rate of change of the flow rule as given in Eq. 3.35 and h' is the hardening as given in Eq. 3.37.

$$\dot{\lambda} = \frac{(\frac{\delta F}{\delta \sigma} : C_m) : (\frac{\delta F}{\delta \sigma} : C_m)}{\frac{\delta F}{\delta \sigma} : (C_m : \frac{\delta F}{\delta \sigma}) + h'} \tag{3.29}$$

The change in the stress in the matrix is related to the elasto-visco-plastic constitutive law, $C_{m_{ep}}$, as given as in Eq. 3.30.

$$\triangle \sigma_m = C_{m_{ep}} \triangle \varepsilon_m \tag{3.30}$$

where $C_{m_{ep}}$ is given as Eq. 3.31.

$$C_{m_{ep}} = C_m - \dot{\lambda} \tag{3.31}$$

3.2.1 Drucker-Prager Flow Rule and Yield Criterion

In order to determine whether the matrix material has yielded, or behaved plastically, a yield criterion is used. The Drucker-Prager flow rule used in this formulation was based on the generalized Von Mises flow rule. Von Mises yield can be defined as in Eq. 3.32.

$$F = \sigma_y = \sqrt{\left(\frac{1}{2}\right)\left[(\sigma_{11}-\sigma_{22})^2 + (\sigma_{22}-\sigma_{33})^2 + (\sigma_{33}-\sigma_{11})^2 - 6(\sigma_{12}^2+\sigma_{23}^2+\sigma_{31}^2)\right]} \tag{3.32}$$

The Drucker-Prager yield criterion modifies the Von Mises criterion by adding a pressure sensitivity term, and is given in Eq. 3.33, where α_m is the pressure sensitivity of the matrix.

$$F = F + \alpha_m I_1 \tag{3.33}$$

where, in tensor notation, I_1 is the first invariant of stress, as seen in Eq. 3.34

$$I_1 = \sigma_{kk} \tag{3.34}$$

The partial derivatives of F are shown in Eq. 3.35.

$$\frac{\delta F}{\delta \sigma_{11}} = 2(\sigma_{11}-\sigma_{22}) - 2(\sigma_{33}-\sigma_{11}) + \alpha_m \tag{3.35a}$$

$$\frac{\delta F}{\delta \sigma_{22}} = 2(\sigma_{22}-\sigma_{33}) - 2(\sigma_{11}-\sigma_{22}) + \alpha_m \tag{3.35b}$$

$$\frac{\delta F}{\delta \sigma_{33}} = 2(\sigma_{33}-\sigma_{11}) - 2(\sigma_{22}-\sigma_{33}) + \alpha_m \tag{3.35c}$$

$$\frac{\delta F}{\delta \sigma_{12}} = 12\sigma_{12} \tag{3.35d}$$

$$\frac{\delta F}{\delta \sigma_{23}} = 12\sigma_{23} \tag{3.35e}$$

$$\frac{\delta F}{\delta \sigma_{31}} = 12\sigma_{31} \tag{3.35f}$$

3.2.2 Ludwik Hardening Law

Hardening is given by the Ludwik equation, given in Eq. 3.36. σ_{ym} is the yield stress of the matrix, K_m is the matrix hardening modulus, ε_m^{pl} is the plastic strain in the matrix material and N_m is the matrix hardening exponent.

$$h' = \sigma_{ym} + K_m(\varepsilon_m^{pl})^{N_m} \tag{3.36}$$

Strain-Rate Sensitivity

As discussed in Section 2.3.3, the matrix has strain-rate sensitivity, so the rate effects were incorporated, as seen in Eq. 3.37. $\dot{\varepsilon}_m$ is the strain rate of the matrix material, $\dot{\varepsilon}_o$ is a reference strain rate, and hm is the strain rate exponent. This approach of using these hardening and strain-rate laws is also investigated in research by Hsu et al. [39].

$$h' = (\sigma_{ym} + K_m(\varepsilon_m^{pl})^{N_m})\left(\frac{\dot{\varepsilon}_m}{\dot{\varepsilon}_o}\right)^{hm} \tag{3.37}$$

3.3 Homogenization

Homogenization is necessary to generalize the behaviour of a heterogeneous material, as mentioned in Section 2.3.1. The Mori-Tanaka approach [54] is implemented based on the general formulation given in the work by Perdahcioglu and Geijselaers [62]. This work is more mathematical than physical, though it still provides a good solution [17]. The formulation for the forward strain concentration tensor, $\mathbb{T}$, is given in Eq. 3.38, where I is the identity matrix, and C_f and C_m are the constitutive matrices for the fibre and matrix respectively, as given in Eqs. 3.26 and 3.25.

$$\overrightarrow{\mathbb{T}} = \left[I + \mathbb{S}\left[C_{m_{ep}}^{-1}(C_f - C_{m_{ep}})\right]\right]^{-1} \tag{3.38}$$

$\mathbb{S}$ in this thesis is the Eshelby tensor for long fibres, and is given in Eq. 3.39, where it is a function of the Poisson's ratio for the matrix material.

$$\mathbb{S} = \begin{bmatrix} 0 & 0 & 0 & 0 & 0 & 0 \\ \frac{\nu_m}{2-2\nu_m} & \frac{5-4\nu_m}{8-8\nu_m} & \frac{4\nu_m-1}{8-8\nu_m} & 0 & 0 & 0 \\ \frac{\nu_m}{2-2\nu_m} & \frac{4\nu_m-1}{8-8\nu_m} & \frac{5-4\nu_m}{8-8\nu_m} & 0 & 0 & 0 \\ 0 & 0 & 0 & \frac{1}{4} & 0 & 0 \\ 0 & 0 & 0 & 0 & \frac{3-4\nu_m}{8-8\nu_m} & 0 \\ 0 & 0 & 0 & 0 & 0 & \frac{1}{4} \end{bmatrix} \tag{3.39}$$

This solution is most applicable for materials where there is a low volume fraction of fibres within the matrix. Oppositely, this solution is applied for high volume fractions if the backwards concentration tensor is calculated, as seen in Eq. 3.40.

$$\overleftarrow{\mathbb{T}} = \left[I + \mathbb{S}\left[C_f^{-1} (C_{m_{ep}} - C_f) \right] \right]^{-1} \tag{3.40}$$

These two solutions are used together through the Lielens interpolation method [62], which allows the Mori-Tanaka homogenization scheme to be applied for materials with intermediate volume fractions. To do this, a Mori-Tanaka constant is introduced as input and is denoted as MTc. This MTc constant is input to the simulation as a matrix where the constant is applied on the terms 1 through 3, as shown in Eq. 3.41.

$$MTc = \begin{bmatrix} MTc & MTc & MTc & 0 & 0 & 0 \\ MTc & MTc & MTc & 0 & 0 & 0 \\ MTc & MTc & MTc & 0 & 0 & 0 \\ 0 & 0 & 0 & 0 & 0 & 0 \\ 0 & 0 & 0 & 0 & 0 & 0 \\ 0 & 0 & 0 & 0 & 0 & 0 \end{bmatrix} \tag{3.41}$$

Rather than calculating the fibre strain through $\mathbb{T}$ as in Eq. 3.1, the strain is interpolated through the forward and backward Mori-Tanaka approach as in Eq. 3.42.

$$\varepsilon_f = \mathbb{A}\varepsilon \tag{3.42}$$

where $\mathbb{A}$ is as shown in Eq. 3.43.

$$\mathbb{A} = \left[(1 - MTc)\overleftarrow{\mathbb{T}}^{-1} + MTc\overrightarrow{\mathbb{T}}^{-1} \right]^{-1} \tag{3.43}$$

3.4 Failure Criterion

The implementation of failure in this model uses the Chang and Chang Failure Criteria, as mentioned in Ch. 2.4.1, which is a stress-based criteria. Once the partitioned stresses are found for the fibre and matrix material, the overall stresses for the composite material are calculated. These stresses are compared against the strength of the material using the Chang and Chang criteria. If any criteria is met, then the material is said to have failed in that direction.

3.5 UMAT Algorithm

The equations given within Chapter 3 needed to be implemented in a user-defined material model in order to be solved numerically. The algorithm that the numerical solver follows is outlined below.

1. Initialize all variables
2. Load any stored variables, such as previous stress and strain increments
3. Calculate C_f and C_m matrices
4. Calculate Eshelby tensor $\mathbb{S}$ (Eq. 3.39)
5. Perform Mori-Tanaka algorithm and return stress (Sect. 3.5.1)
6. Calculate failure criteria (Eq. 2.17, Eq. 2.18 and Eq. 2.19)
7. Compare stress to failure criteria and fail material as needed
8. Save variables, such as all stress and strain increments

3.5.1 Mori-Tanaka Algorithm

In the above sections, the constitutive equations were given for the total stresses and strains. When implemented in the numerical simulation, the incremental stresses and strains were used. The steps in the Mori-Tanaka algorithm are as follows.

1. Set $\mathbb{T} = 0$
2. Calculate initial Forward and Backward Mori-Tanaka tensors $\overrightarrow{\mathbb{T}}$, $\overleftarrow{\mathbb{T}}$ (Eq. 3.38, Eq. 3.40) and $\mathbb{A}$ (Eq. 3.43)

$$\overrightarrow{\mathbb{T}} = \left[I + \mathbb{S}\left[C_{m_{ep}}^{-1} (C_f - C_{m_{ep}}) \right] \right]^{-1}$$

$$\overleftarrow{\mathbb{T}} = \left[I + \mathbb{S}\left[C_f^{-1} (C_{m_{ep}} - C_f) \right] \right]^{-1}$$

$$\mathbb{A} = \left[(1 - MTc)\overleftarrow{\mathbb{T}}^{-1} + MTc\overrightarrow{\mathbb{T}}^{-1} \right]^{-1}$$

3. Strain partitioning

   (a) Modify volume fraction (Eq. 3.24)

$$V_{fe} = \frac{V_f}{900}\left[480m\left(l^2 - k^2\right) + 30l^2 + 360kl + 510k^2\right]$$

   (b) Calculate incremental fibre strain (Eq. 3.42)

$$\triangle\varepsilon_f^{(t)} = \triangle\varepsilon_f^{(t-1)} + \mathbb{A}\triangle\varepsilon^{(t)}$$

   (c) Calculate incremental matrix strain (Eq. 3.7)

$$\triangle\varepsilon_m^{(t)} = \triangle\varepsilon^{(t)} - \frac{\triangle\varepsilon_f^{(t)}(V_{fe})}{1 - V_{fe}}$$

4. Stress Calculation

   (a) Calculate incremental fibre stress (Eq. 3.2)

$$\triangle\sigma_f^{(t)} = \triangle\sigma_f^{(t-1)} + C_f\triangle\varepsilon_f^{(t)}$$

   (b) Calculate incremental matrix stress (Eq. 3.11)

      i. Calculate initial trial stress

$$\triangle\sigma_m^{(t)} = \triangle\sigma_m^{(t-1)} + C_m\varepsilon_m^{(t)}$$

$$\sigma_{mt}^{(t)} = \sigma_m^{(t)} + \triangle\sigma_m^{(t)}$$

      ii. Calculate trial matrix strain rate

$$\dot{\varepsilon}_m^{(t)} = \sqrt{\frac{\frac{2}{3}(\varepsilon_m^{(t)})(\varepsilon_m^{(t)})}{\triangle t}}$$

      iii. Calculate yield and hardening (Eq. 3.33, Eq. 3.37)

$$F = F + \alpha_m I_1$$

$$h' = (\sigma_{ym} + K_m(\varepsilon_m^{pl})^{N_m})\left(\frac{\dot{\varepsilon}_m}{\dot{\varepsilon}_o}\right)^{hm}$$

iv. Check for plasticity. If plastic deformation occurs

A. Calculate tangent modifier

$$\dot{\lambda} = \frac{(\frac{\delta F}{\delta \sigma} : C_m) : (\frac{\delta F}{\delta \sigma} : C_m)}{\frac{\delta F}{\delta \sigma} : (C_m : \frac{\delta F}{\delta \sigma}) + h'}$$

B. Calculate the temporary stress in the matrix

$$\sigma_{mt}^{(t)} = \sigma_{mt}^{(t)} - \dot{\lambda} C_m \frac{dF}{d\sigma}$$

C. Calculate yield and hardening (Eq. 3.33, Eq. 3.37)

$$F = F + \alpha_m I_1$$

$$h' = (\sigma_{ym} + K_m (\varepsilon_m^{pl})^{N_m}) \left(\frac{\dot{\varepsilon}_m}{\dot{\varepsilon}_o} \right)^{hm}$$

D. Return to 4(b)iv until plastic step < tolerance

v. Calculate final tangent modifier

$$\dot{\lambda} = \frac{(\frac{\delta F}{\delta \sigma} : C_m) : (\frac{\delta F}{\delta \sigma} : C_m)}{\frac{\delta F}{\delta \sigma} : (C_m : \frac{\delta F}{\delta \sigma}) + h'}$$

vi. Calculate the plastic matrix

$$C_{m_{ep}} = C_m - \dot{\lambda}$$

vii. Calculate stress increment for current iteration

$$\triangle \sigma_m^{(t)} = C_{m_{ep}} \triangle \varepsilon_m^{(t)}$$

viii. Recalculate initial Forward and Backward Mori-Tanaka tensors $\overrightarrow{\mathbb{T}}$, $\overleftarrow{\mathbb{T}}$ (Eq. 3.38, Eq. 3.40) and $\mathbb{A}$ (Eq. 3.43)

(c) Calculate error

$$\varepsilon_{temp}^{(t)} = \varepsilon_{temp}^{(t)} + \mathbb{A}^{-1} \triangle \varepsilon_f^{(t)}$$

$$RESID = RESID + \sqrt{(\varepsilon^{(t)} - \varepsilon_{temp}^{(t)})(\varepsilon^{(t)} - \varepsilon_{temp}^{(t)})}$$

(d) Return to 3 until RESID < tolerance

5. Average stress

   (a) Calculate stress in fibre

   $$\sigma_f = \sigma_f + \triangle\sigma_f$$

   (b) Calculate stress in matrix

   $$\sigma_m = \sigma_m + \triangle\sigma_m$$

   (c) Calculate strain in fibre

   $$\varepsilon_f = \varepsilon_f + \triangle\varepsilon_f$$

   (d) Calculate strain in matrix

   $$\varepsilon_m = \varepsilon_m + \triangle\varepsilon_m$$

   (e) Calculate homogenized total stress

   $$C_{avg} = V_{fe}(C_f - C_{m_{ep}})\mathbb{A} + C_{m_{ep}}$$

   $$\sigma = \sigma + C_{avg}\varepsilon$$

3.6 Limitations

One limitation of this model is that the strain concentration tensor, $\mathbb{T}$, is only able to be calculated based on the work by Eshelby for a composite with only two phases since the inclusion theory was developed for the case of one inclusion being imbedded in an infinite matrix material [62]. However, research is being done in this field to further extend Eshelby's model.

The Mori-Tanaka approach has some limitation when used for large deformations due to the averaging principle, but if it is implemented in an incremental approach, as was done in this UMAT, then the results are approximately correct [62]. As well, the Mori-Tanaka homogenization scheme does not take into account fibre-fibre interactions, the effect of which is more prominent with higher volume fraction materials.

Chapter 4

Results

This chapter provides and discusses the simulated results in comparison with experimental data from literature. Two sets of data are provided to validate the model's performance for plasticity. Experimental data showing the strain rate dependency of the overall composite is compared against simulation results. A parametric study shows the effect of the k, l and m pairing parameters from the micromechanics formulation, as well as the calibration parameters for the plasticity model.

4.1 Simulation and UMAT Setup

The constitutive laws given in Section 3 are implemented into a user-defined material model (UMAT), MAT_042 in LS-DYNA. As input, the material parameters provided in Tables 4.2 and 4.3 are used for two different carbon fibre/epoxy models.

A single brick element, shown in Figure 4.1, is used, where each side is 20 mm long. The boundary card *BOUNDARY_SPC_SET is used to set boundary conditions on the element in order to perform tension, compression and shear tests. Tension and compression tests are performed in the x-direction (axial) and the y-direction (transverse) as the material is transversely isotropic. The *BOUNDARY_SPC_SET fixed translation and rotation on a face for a given loading case. The *BOUNDARY_PRESCRIBED_MOTION_SET allows the user to input a load curve with which a velocity is prescribed to pull or compress the element as needed.

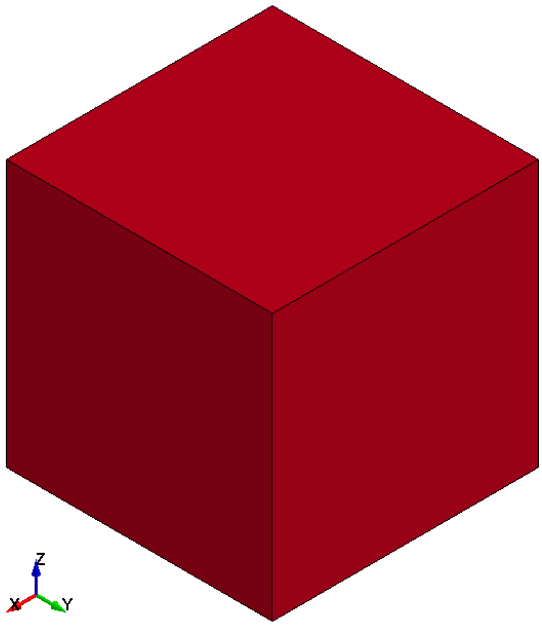

Figure 4.1: Single solid element

4.2 Elastic Results

In order to determine the accuracy of this model, it was compared with tensile and compressive data from Kyriakides et al. [47]. This work examines the failure mechanisms of unidirectional fibre composites under compression with a APC-2/AS4 composite. APC-2 is a PEEK thermoplastic and AS4 is a high strength and high strain carbon fibre.

As input to the model, the material data for the fibre and the matrix is used, as well as the overall strengths of the composite material. The constituent properties were taken from Kyriakides et al.[47], where the strengths were taken from Carlile et al. [11], and corroborated with online data sheets [18].

Table 4.1 shows the material data, where E_m and ν_m are the elastic constant and the Poisson's ratio for the matrix. E_{fa} and E_{ft} are the elastic modulus for the fibre in the axial and transverse direction, respectively. In addition, ν_{fta} and ν_{ft} are the Poisson's ratio for the fibre in the transverse axial and transverse direction. V_f is the fibre volume fraction and G_f is the shear modulus for the fibre. k, l and m are pairing constants which determine the bounds on the interphase zone.

To determine failure in the material, X_t, X_c, Y_t, Y_c, S_c and α are used. X_t and X_c are the longitudinal strengths in tension and compression, and Y_t and Y_c are the transverse strengths in tension and compression. S_c is the shear strength, and α is an experimentally determined parameter.

Table 4.1: Elastic Material and Calibration Data for APC-2/AS4 Composite [11, 18, 47]

E_{m} (GPa)	ν_{m}	E_{fa} (GPa)	E_{ft} (GPa)	ν_{fta}	ν_{ft}	G_{f} (GPa)	V_{f}	α
4.10	0.356	214.0	26.0	0.28	0.445	112.0	0.6	0.3

X_{t} (GPa)	X_{c} (GPa)	Y_{t} (GPa)	Y_{c} (GPa)	S_{c} (GPa)	k	l	m
1.37	1.2	0.079	0.214	0.136	0.9	1.15	0.4

The experimental and simulated results in elasticity are shown in Figure 4.2. It is seen that the simulation of longitudinal tension is in very good agreement with the experimental data. Since fibres primarily behave elastically, this follows from theory. In transverse tension, the simulation deviates from the experimental data slightly, while simulated compression in the axial direction begins to differ from the experimental data after 0.3%. In the transverse direction, the deviation becomes quite pronounced after about 1.6% strain.

It is clear in compression, and in the transverse directions, that plasticity of the matrix material does indeed play a strong role. In order to be able to accurately predict composite behaviour, plasticity must be implemented.

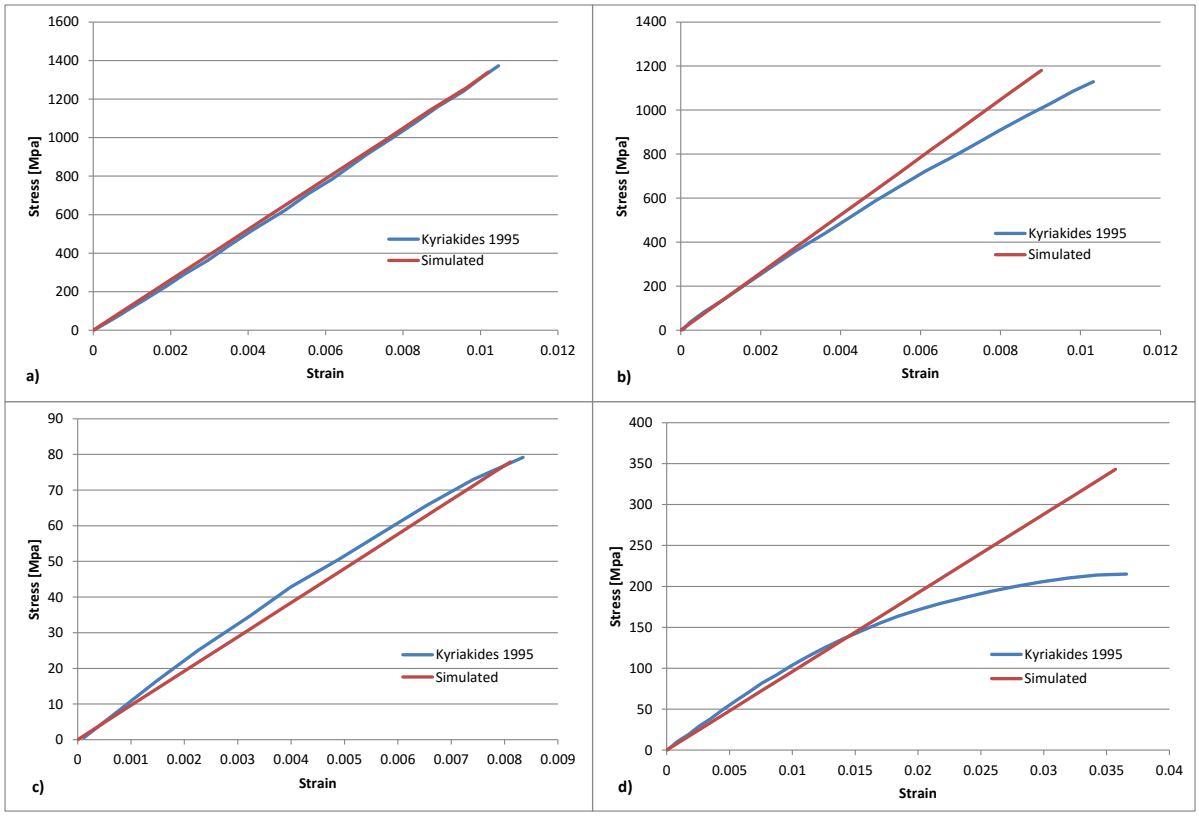

Figure 4.2: Elastic Experimental vs. Simulated Results for a) longitudinal tension b) longitudinal compression c) transverse tension d) transverse compression [45]

4.3 AS4/APC-2 Plastic Results

The same set of data from Kyriakides et al. [47] is used again once visco-plasticity is implemented in the model. Table 4.2 shows the input material parameters for the visco-plastic formulation. In this table, K_m is the matrix hardening modulus, N_m is the matrix hardening exponent, and σ_{ym} is the yield stress of the matrix. α_m is the pressure sensitivity of the matrix, and hm and $\dot{\varepsilon}_o$ are the rate sensitivity parameters for the matrix material.

Table 4.2: Plastic Material and Calibration Data for APC-2/AS4 Composite [11, 18, 38, 47]

E_{m} (GPa)	ν_{m}	E_{fa} (GPa)	E_{ft} (GPa)	ν_{fta}	ν_{ft}	G_{f} (GPa)	V_{f}	α
4.10	0.356	214.0	26.0	0.28	0.445	112.0	0.6	0.3

X_{t} (GPa)	X_{c} (GPa)	Y_{t} (GPa)	Y_{c} (GPa)	S_{c} (GPa)	k	l	m	MTc
1.37	1.2	0.079	0.214	0.136	0.8	1.15	0.45	0.77

K_{m} (GPa)	N_{m}	σ_{ym} (GPa)	α_{m}	hm	$\dot{\varepsilon}_o$
137.0	0.1	5.0	0.1415	0.02	6e-7

The transverse compression direction is used to calibrate the model against the experimental data. Figure 4.3 shows the results from the quasi-static simulation compared to experimental data. The experimental data from the Kyriakides paper gives the transverse strain up to 4%. The hardening modulus, exponent and yield stress of the matrix are modified, along with the interphase pairing parameters in order to produce a good fit to the experimental data along the entire length of the curve.

It is seen that the simulated curve underpredicts the experimental results until about 1.7% strain, whereas the agreement following that strain value is good until the material fails. As well, the experimental data is fairly linear in behaviour below 1% strain. The simulated results are able to capture this behaviour, although they deviate slightly from the exact experimental results. The simulated model underpredicts the stress by about 7%. As well, the elastic stress-strain curve shown in part d of Figure 4.2 are compared against the elasto-visco-plastic results, since this loading case shows the greatest deviation from the experimental results. It is clear that incorporating the elasto-visco-plastic framework into the constitutive model allows for a more accurate prediction of the experimental results.

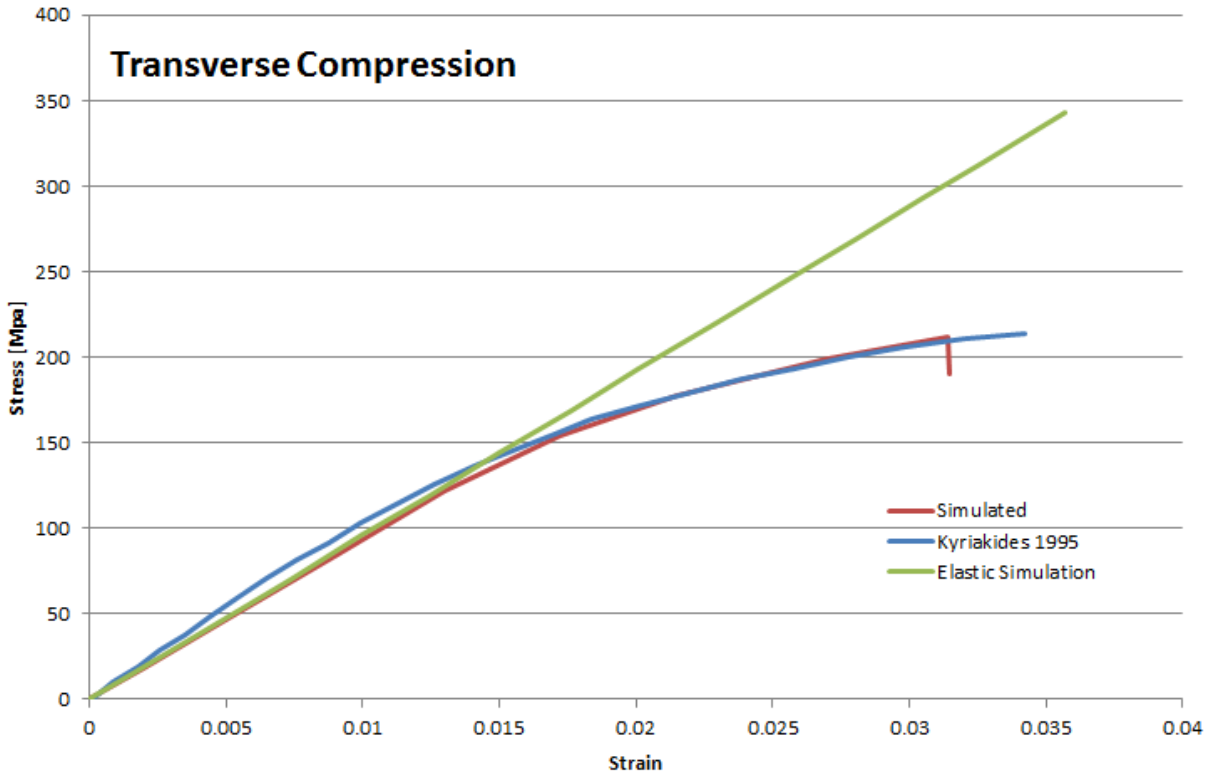

Figure 4.3: Transverse compression calibration simulation compared with experimental data and elastic simulation [47]

Once the transverse compression curve is calibrated, tension and compression simulations are run in both the transverse and longitudinal directions to predict the material response. These graphs are shown in Figures 4.4, 4.5, 4.6 and 4.7.

The simulated result in Figure 4.4 also shows very good agreement with the experimental data. At 0.8% strain, the simulation underpredicts by 5%. Progressive interface debonding plays a role in damage, especially when a unidirectional material is loaded in transverse tension [77]. To date, this behaviour is not captured in the simulated model, which results in a linear behaviour. Failure occurs at a slightly higher strain in the simulation than it does in this set of experimental data.

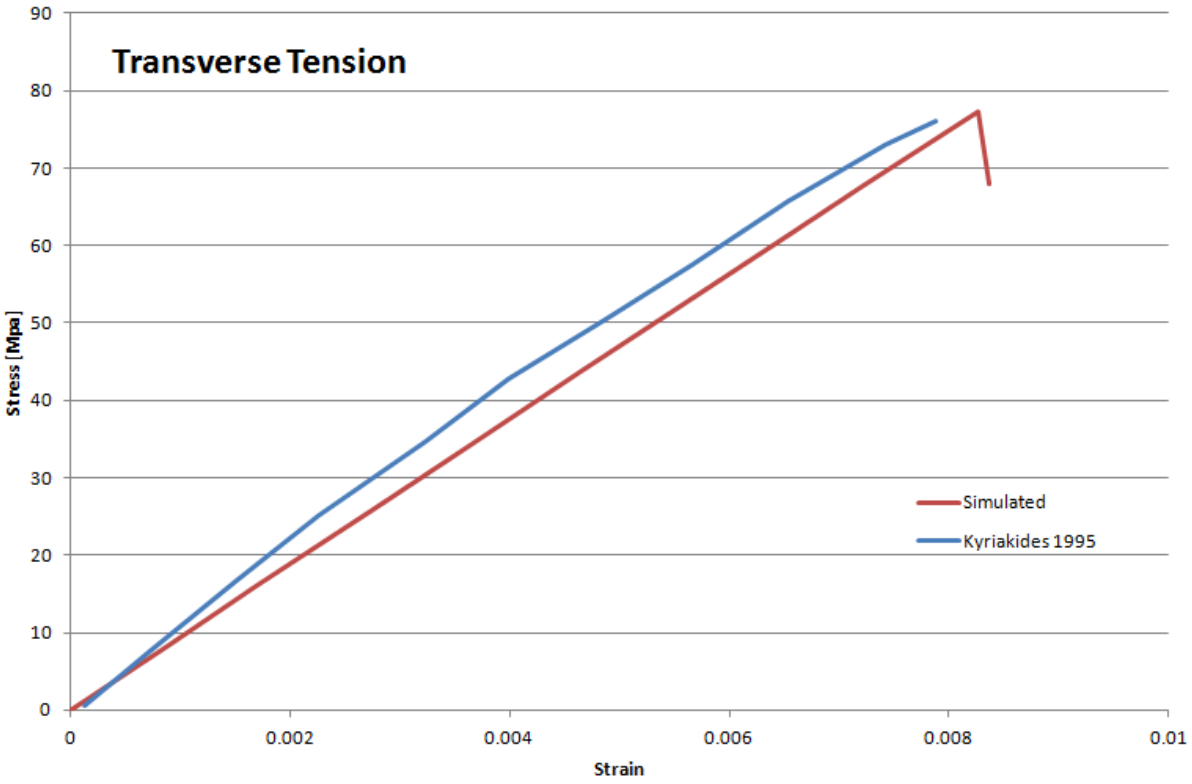

Figure 4.4: Transverse tension simulation compared with experimental data [47]

In longitudinal compression, the simulation shows strong agreement to the experimental data, as seen in Figure 4.5, though the model overpredicts after 0.5% strain. The simulated results fail at a lower strain and higher stress than the experimental data. This is likely due to the fact that fibre imperfections play a role in the compressive strength and behaviour [47], and there is consequently a large spread in the overall strenght values. Unidirectional materials fail in longitudinal compression due in part to the development of kink bands in the material [47], which is illustrated in the softening of the experimental curve, and this phenomenon is not yet captured by the simulated model. The difference in failure strain in the simulation is 10% and the difference in failure stress is 4%, or 52 MPa.

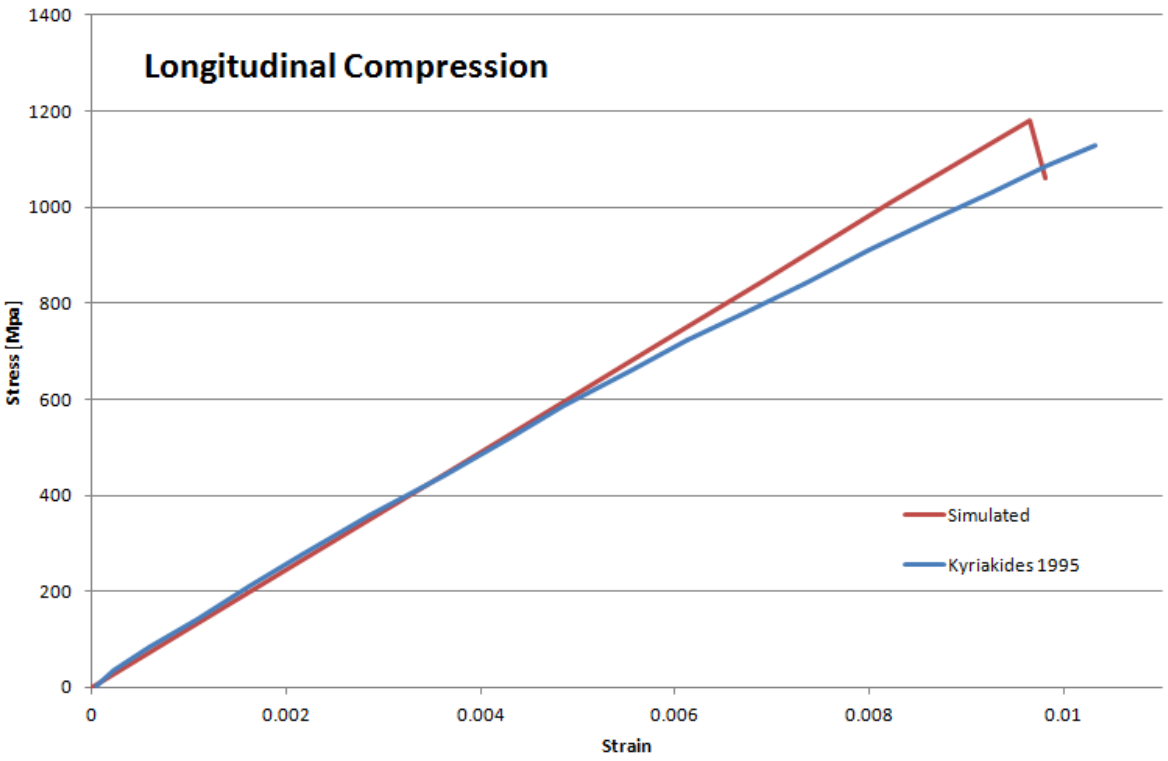

Figure 4.5: Longitudinal compression simulation compared with experimental data [47]

In longitudinal tension, the simulation underpredicts by about 6%, as the simulated results are purely elastic. In reality, these fibres are slightly non-linear and stiffen slightly in longitudinal tension due to their lamellar microstructure [47]. As with the behaviour in the longitudinal compression, this micromechanics behaviour is not yet caputured in this model. Failure occurs at 1% strain, though the simulated material response fails at a stress value of 1.23 GPa, whereas the experimental results show failure occuring at a stress of 1.31 GPa, which is still within a range of values for the strength of the material [47].

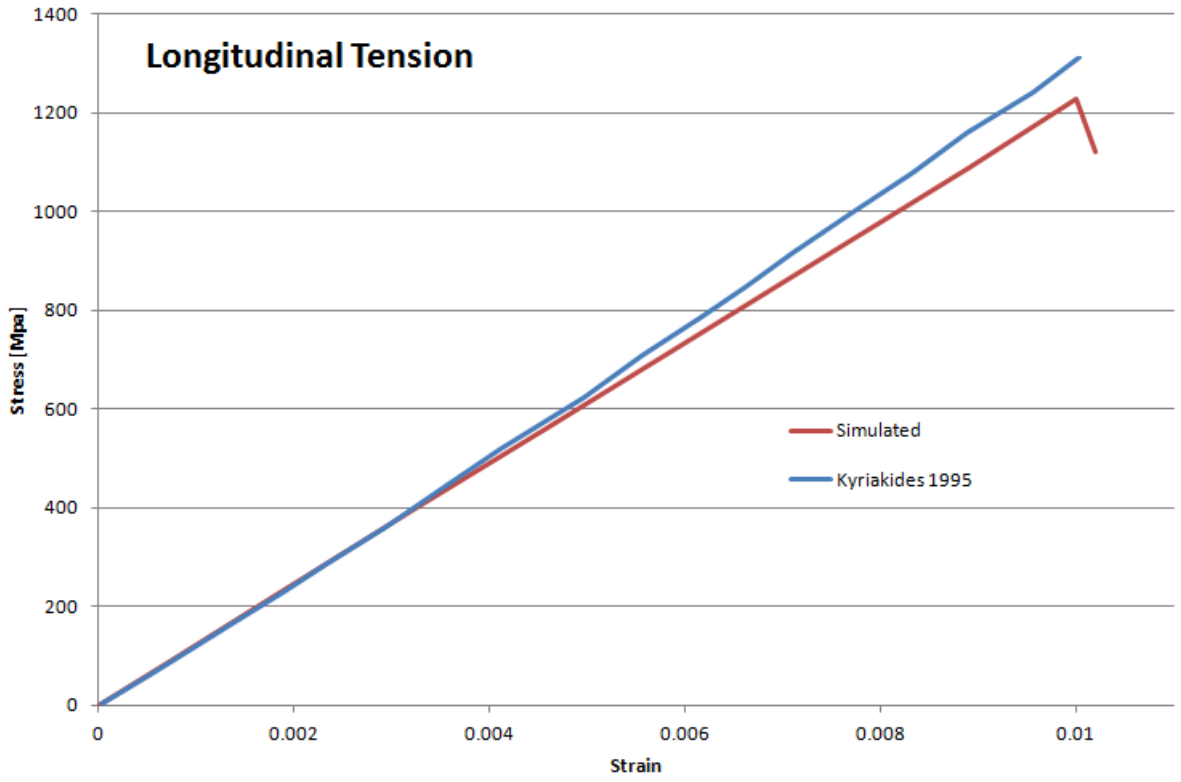

Figure 4.6: Longitudinal tension simulation compared with experimental data [47]

The shear response in the XY-plane is highly non-linear, and this response proved more difficult to accurately capture. The simulated response up to 3.5% strain is shown in Figure 4.7. Experimental results for a unidirectional composite made from AS4/APC-2 are not found, so no comparison is performed with experimental results. It is seen that the simulated response appears linear until about 1.2% strain, then behaves plastically beyond this strain value.

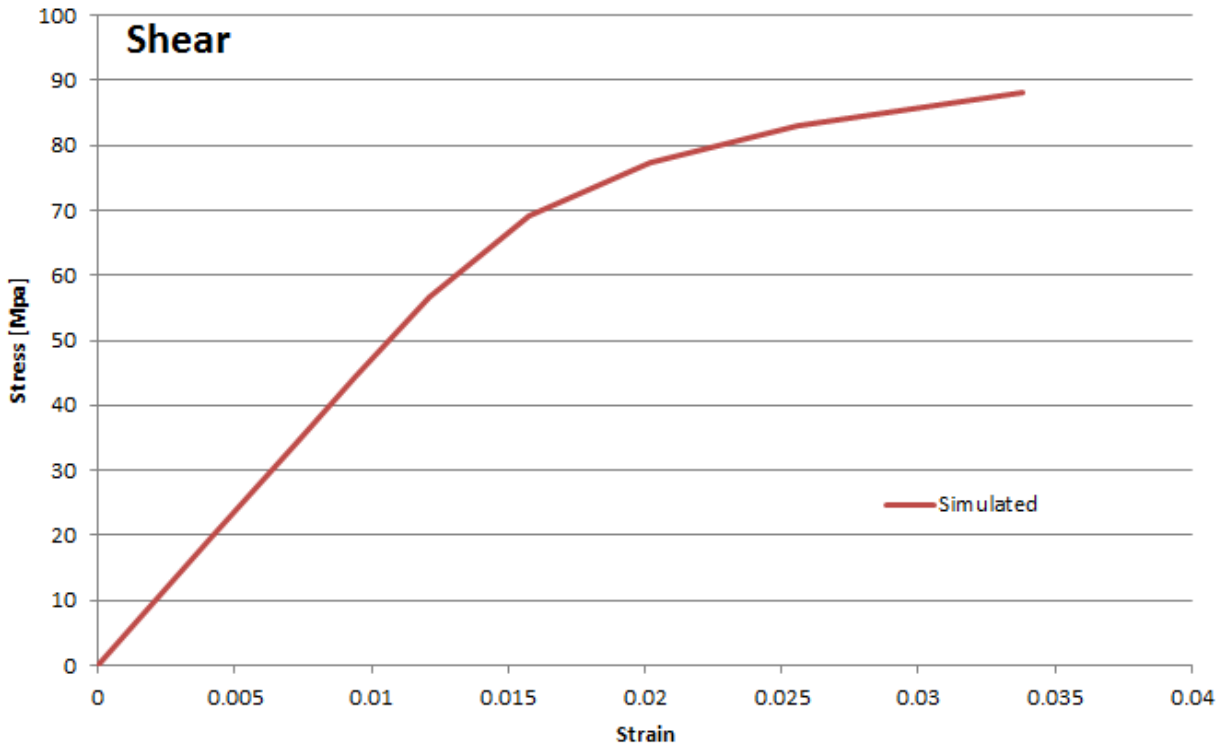

Figure 4.7: XY shear simulation

4.4 IM6G/3501-6 Plastic Results

Elasto-visco-plastic simulations are compared against data from Hsiao and Daniel [36] for the compressive stress-strain curves of a prepreg material, IM6G/3501-6 carbon/epoxy. Because this is a prepreg, it is very difficult to find the fibre properties on their own. Prepreg refers to a special resin matrix system where a number of fibres are already introduced. The strengths of the overall material were taken from Hsiao and Daniel [36], but the constituent properties were taken from elsewhere in literature [43], and are shown in Table 4.3. E_{ft} was taken to be equal to E_{fa} as was done in literature.

Table 4.3: Plastic Material and Calibration Data for IM6G/3501-6 Composite [36, 43]

E_{m} (GPa)	ν_{m}	E_{fa} (GPa)	E_{ft} (GPa)	ν_{fta}	ν_{ft}	G_{f} (GPa)	V_{f}	α
2.31	0.356	279.0	279.0	0.3	0.445	109.0	0.66	0.3

X_{t} (GPa)	X_{c} (GPa)	Y_{t} (GPa)	Y_{c} (GPa)	S_{c} (GPa)	k	l	m	MTc
2.236	1.682	0.0462	0.213	0.0728	0.7	1.15	0.45	0.68

K_{m} (GPa)	N_{m}	σ_{ym} (GPa)	α_{m}	hm	$\dot{\varepsilon}_o$
90.0	0.05	5.0	0.1415	0.02	6e-7

Stress-strain curves from Hsiao and Daniel are given in Figures 4.8, 4.9 and 4.10. Using the same calibration parameters as in the Kyriakides section, the simulated results in Figure 4.8 are calibrated to provide good fit with the experimental data. The results from the Sabiston model are also provided. It is seen that the stress between 1.5% and 2.5% is overpredicted by the simulation, whereas the Sabiston model shows very good agreement. Once strain increases beyond 2%, the Sabiston model begins to deviate from the experimental data, whereas the simulation is able to capture plastic behaviour of the material. Failure in the transverse compression loading case occured at approximately the same stress and strain values for both the experimental data and in the simulation.

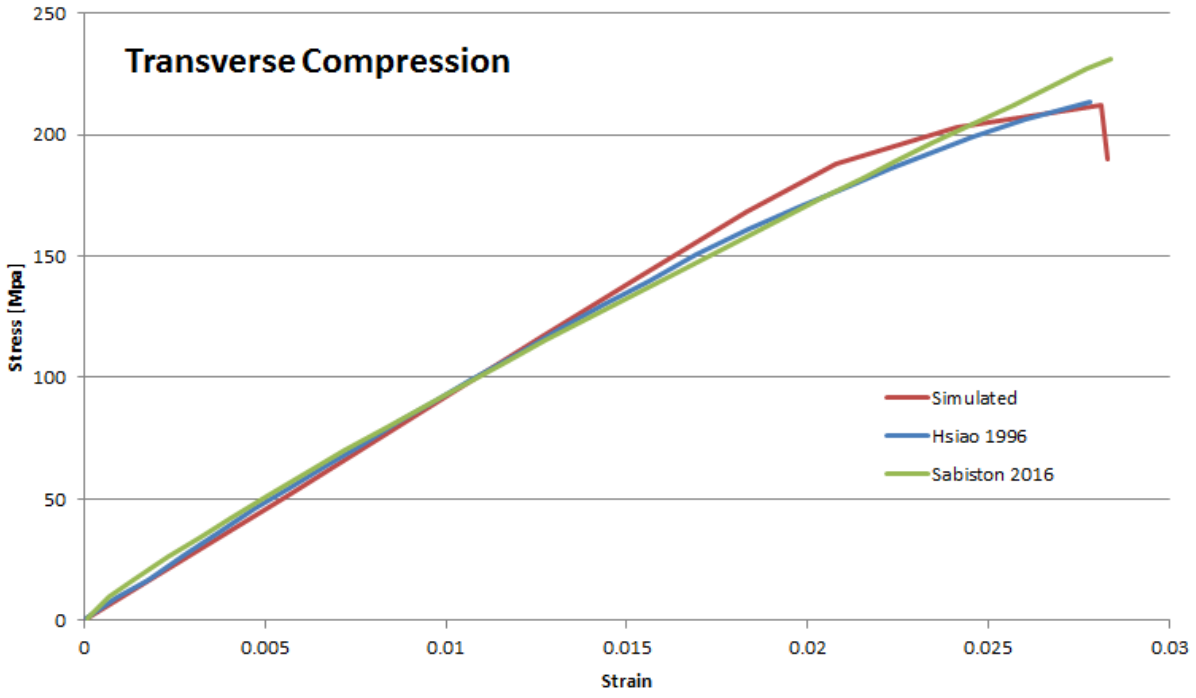

Figure 4.8: Transverse compression calibration simulation compared with experimental data and model from literature [36, 69]

In longitudinal compression, both the simulation and the Sabiston model underpredict strain below 0.8%. After 0.9%, both models overpredict the experimental stress, by a difference of about 3-4%. Failure in the simulation occurs at the same stress as in the experimental results, though the strain values differed by 5%.

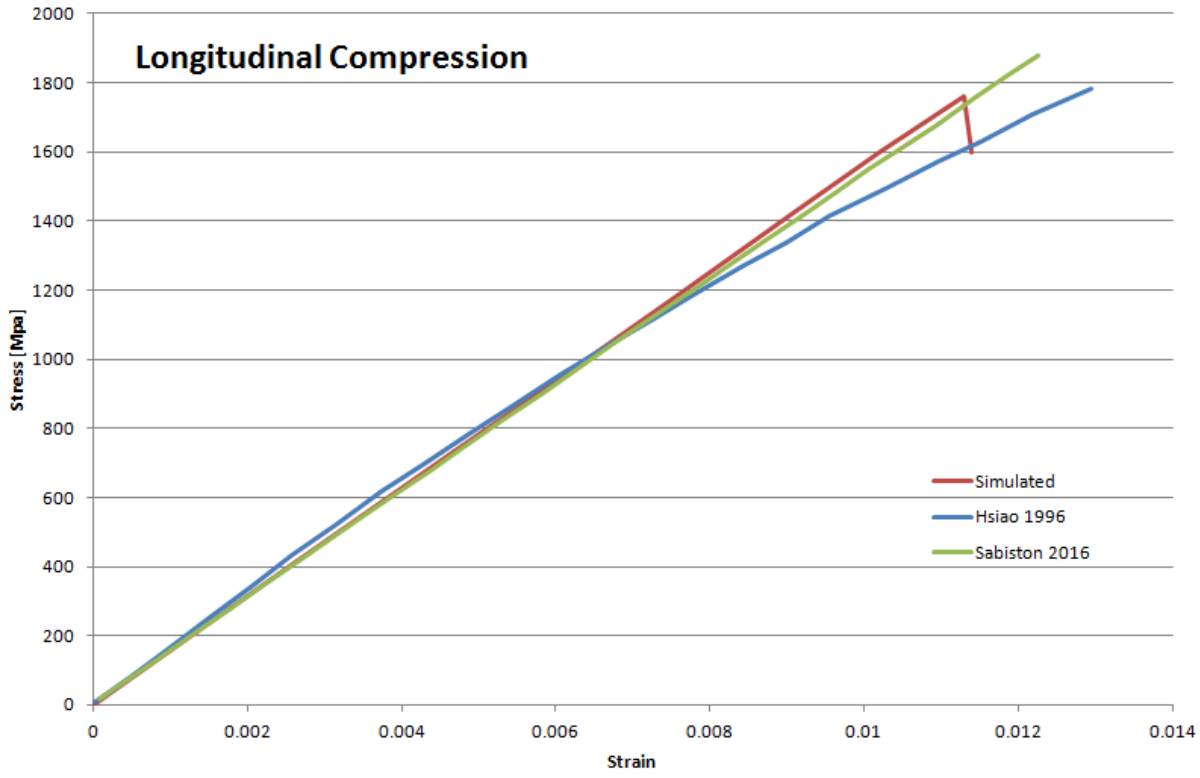

Figure 4.9: Longitudinal compression simulation compared with experimental data and model from literature [36, 69]

As with the XY shear material response in the previous section, the shear response in this material is also highly non-linear. The simulation is able to capture the response of the material though there is underprediction in stress below 1% strain, and overprection of stress above that strain value. The underprediction of a nominal value of 5 MPa, which still lends to good capabilities in response precition. The Sabiston model performs better than the simulated response in this loading case, as it is able to more closely match the experimental data between 0.7% and 1.5%.

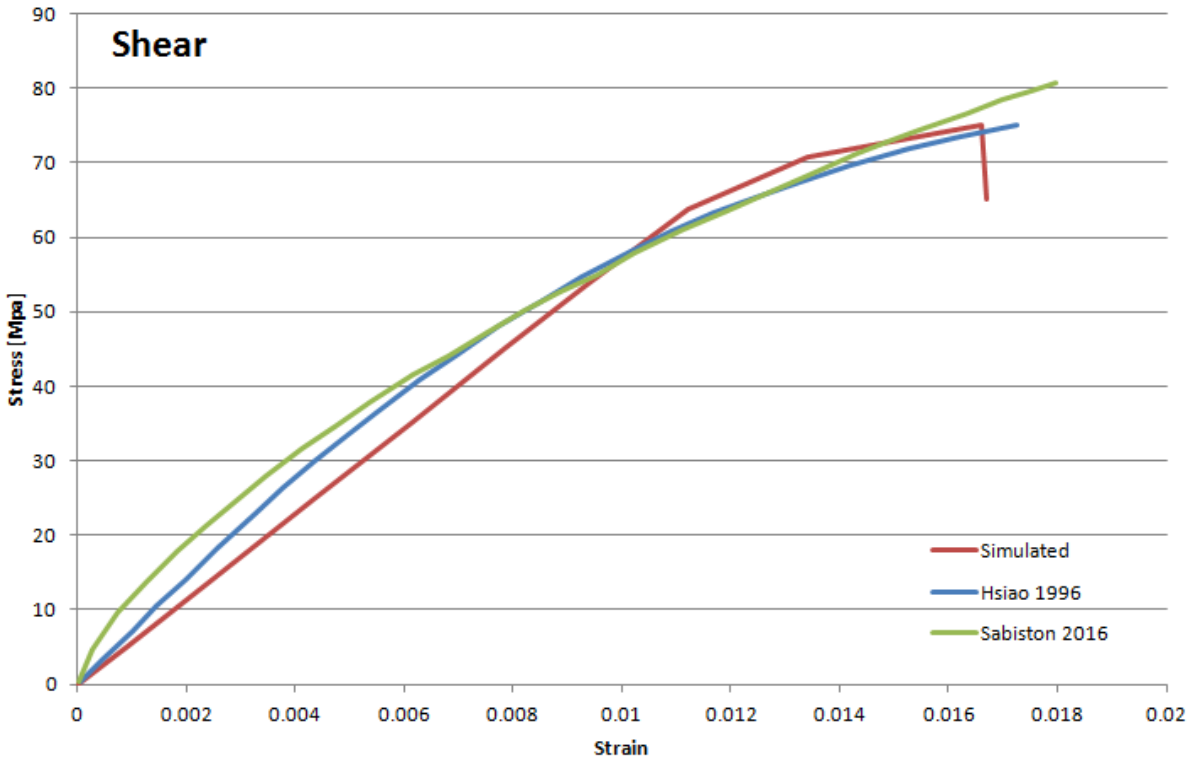

Figure 4.10: XY shear simulation compared with experimental data and model from literature [36, 69]

Overall, these results show that this macroscale model is able to predict the stress-strain response in a similar range of accuracy as the microscale model developed by Sabiston.

4.5 Strain Rate Results

To validate the strain rate prediction of this model, rate dependent experimental data in the transverse compression loading case for the AS4/APC-2 material is used from the pair of papers by Vogler and Kyriakides, and Hsu et al. [38, 83]. The material parameters are as given in 4.2 for low strain rates. However, at high strain rates, k is taken to be 0.9.

A comparison between the experimental results and the numerical simulation is seen in Figure 4.11. A variety of strain rates are run between quasi-static loading (1.5 x 10^{-5} /s) through to 1.5 x 10^{0} /s. It is seen that for each of the four strain rates, the simulated stress-strain curves provide an accurate prediction of the experimental results.

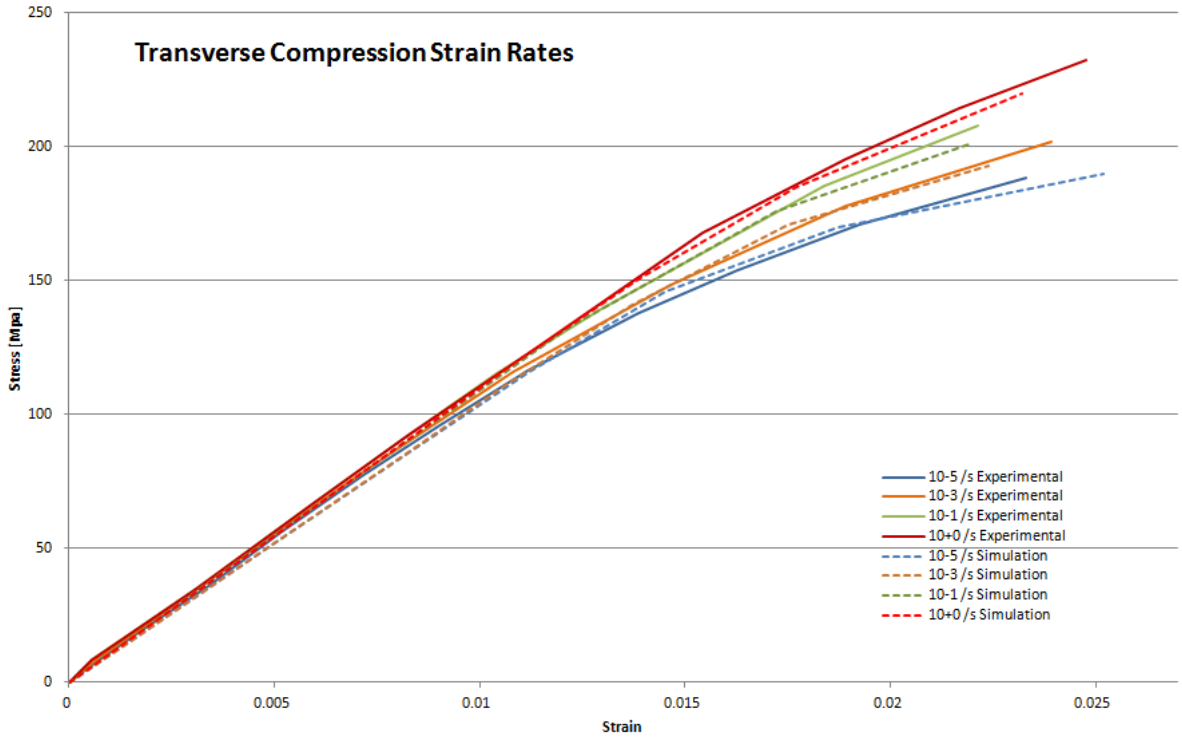

Figure 4.11: Strain rate simulated results compared with experimental results [38, 83]

4.6 Multiple Elements

A specimen with multiple elements is also used to verify that this formulation is able to predict the same results as with a single element, as this is more representative of a full part simulation. A flat coupon is created with dimensions of 196 mm long, 10.26 mm wide and 2.54 mm thick. It is meshed as seen in Figure 4.12 with 50 elements along its length, 4 along its width and 2 in the through-thickness direction, with the fibre direction running along the x-direction.

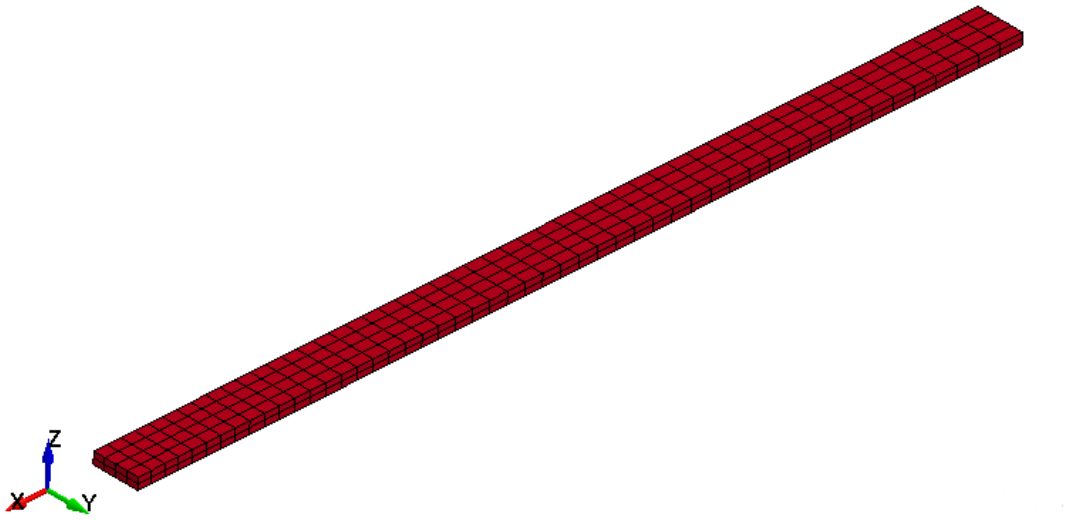

Figure 4.12: Specimen with multiple elements

Figure 4.13 shows a comparison between single and multiple element results for predicted stress-strain graphs in longitudinal tension and transverse compression. In both graphs, the predicted results are identical for both simulations, showing that this formulation is able to perform predicitons with multiple elements.

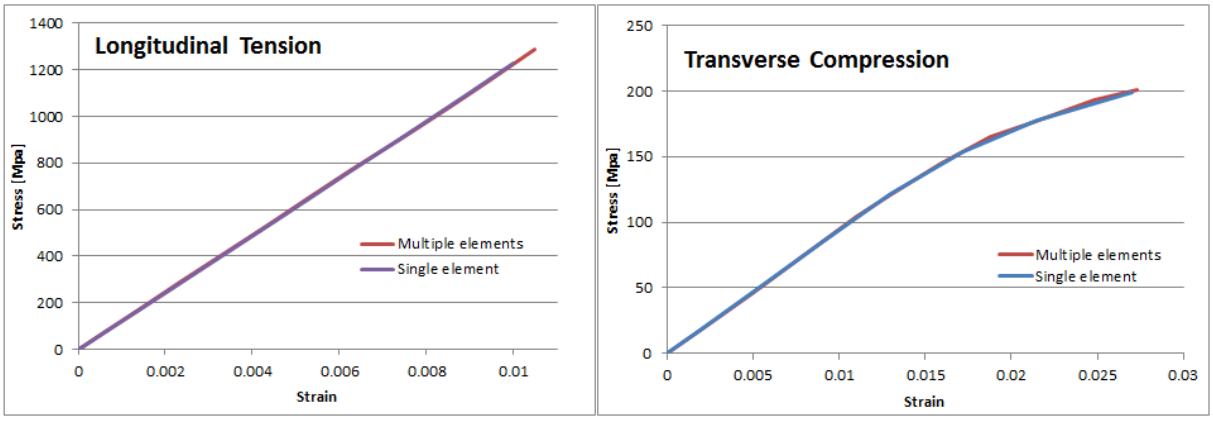

Figure 4.13: Comparison of simulated results between single and multiple elements in longitudinal tension and transverse compression

4.7 Parametric Study

It is imperative to know the effects that the addition of the interphase zone and the corresponding material pairing constants, k, l and m, have on the stress-strain response of the material. Consequently, a parametric study has been performed to investigate these parameters. In addition, having knowledge of how the matrix hardening modulus, K_m, the matrix hardening exponent, N_m and the yield stress of the matrix, σ_{ym} effect the stress-strain response allows the user to more efficiently calibrate the curve for a given material. Lastly, the effect of the Mori-Tanaka constant is discussed.

Figure 4.14 shows the effect of the pairing constant k. This constant effects the inner radius of the interphase zone as seen in Eq. 3.21. It is clear to see the trend that as k increases, the slope of the elastic stress-strain curve increases. This is because the radius of the inner interphase zone increases, tending the material response more toward the fibre behaviour. By varying k between 0 and 1, the stress has the potential to vary by about 50 MPa.

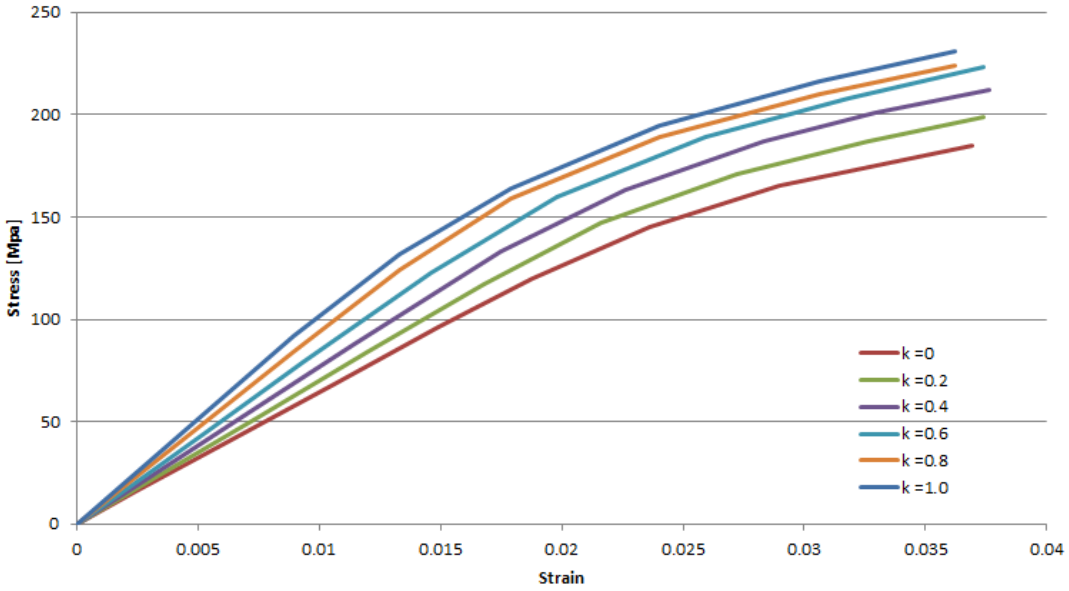

Figure 4.14: Parametric study of k

The effect of the pairing constant l is shown in Figure 4.15. This constant effects the outer radius of the interphase zone, as in Eq. 3.21. Because of the bounds on l shown in Eq. 3.22, there is a much smaller effect on the stress-strain response. For a material with a 60% volume fraction, as with the materials investigated in this thesis, l is bounded between 1 and 1.15. l varies slightly as its value is changed at lower strains, but this effect becomes less pronounced as strain increases above 2.5%. In general, as l increases, the response of the material also increases.

The pairing constant m is used in the calculation of the effective volume fraction, V_{fe}, as seen in Eq. 3.23. Like k, m varies between 0 and 1. Figure 4.16 shows that as m increases in the linear regime, the response of the material also increases. In this region (below 1.5% strain), the stress varies up to about 15 MPa. However, as strain constinues to increase, the effect of m on the material response changes. After about 2% strain, it can be seen that as m increases, the material response decreases.

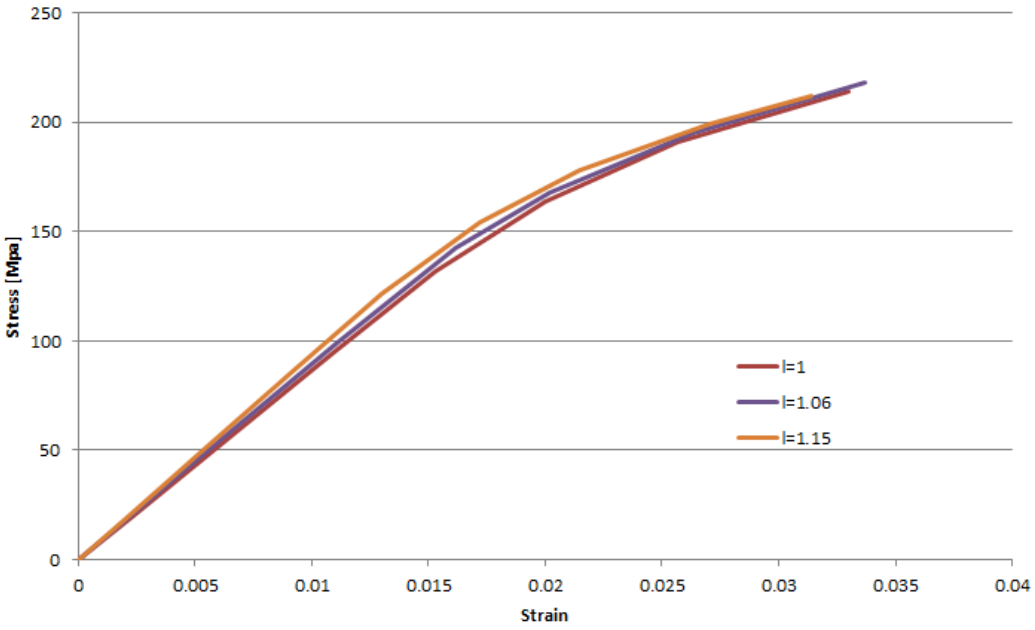

Figure 4.15: Parametric study of l

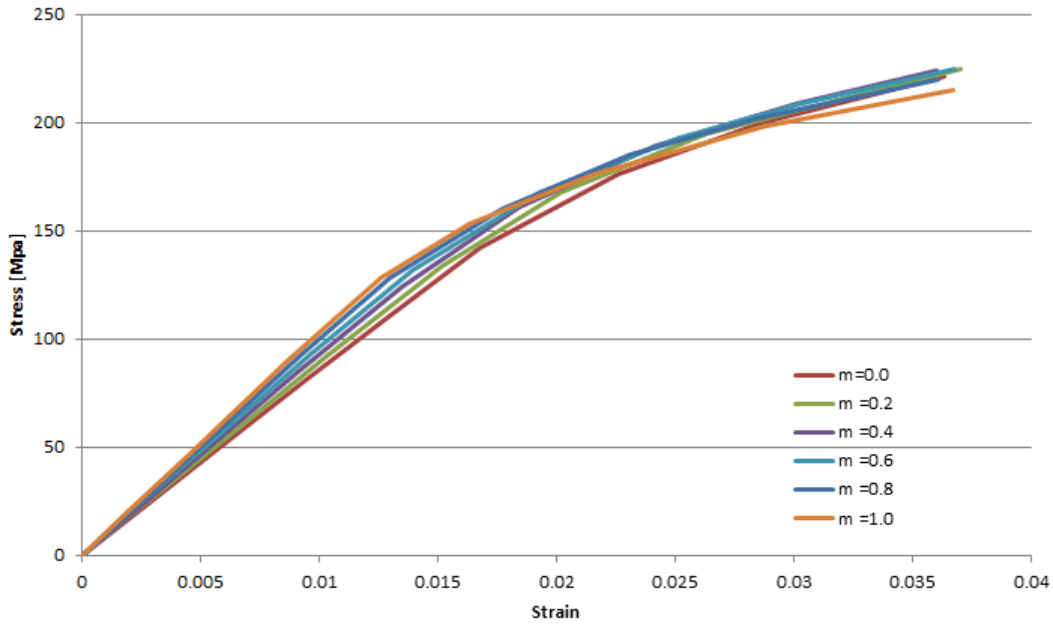

Figure 4.16: Parametric study of m

K_m is the matrix hardening modulus and is used as seen in Eq. 3.36. It can be seen in Figure 4.17 that as K_m increases, both the magnitude of the stress value and the slope of the hardening curve increases. Changing the value of K_m between 10 and 150 results in a change of stress of 190 MPa at 3% strain.

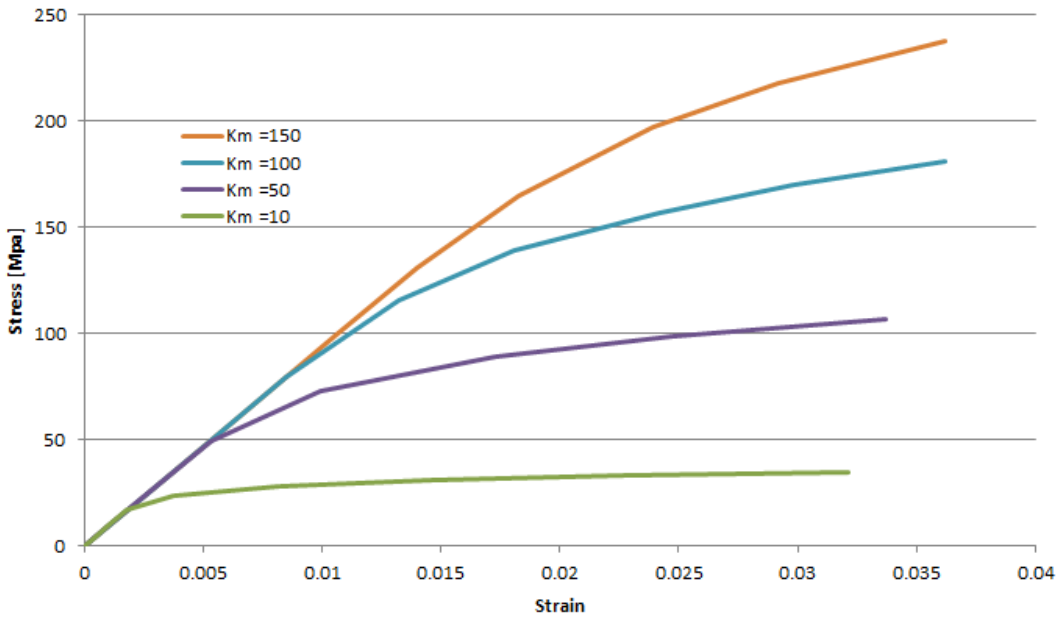

Figure 4.17: Parametric study of K_m

Variation of N_m, the matrix hardening exponent, also changes the stress-strain response. It is seen in Figure 4.18 that increasing N_m decreases the point where the response begins to deviate from the elastic response. N_m was varied between 0.01 and 0.15, and the stress varies by 100 MPa at 3% strain depending on the value of N_m.

The variation of the yield stress of the matrix, σ_{ym}, is shown in Figure 4.19. Increasing σ_{ym} increases the response of the stress-strain curve, which is opposite to that of N_m. σ_{ym} effectively scales the yield point of the matrix material.

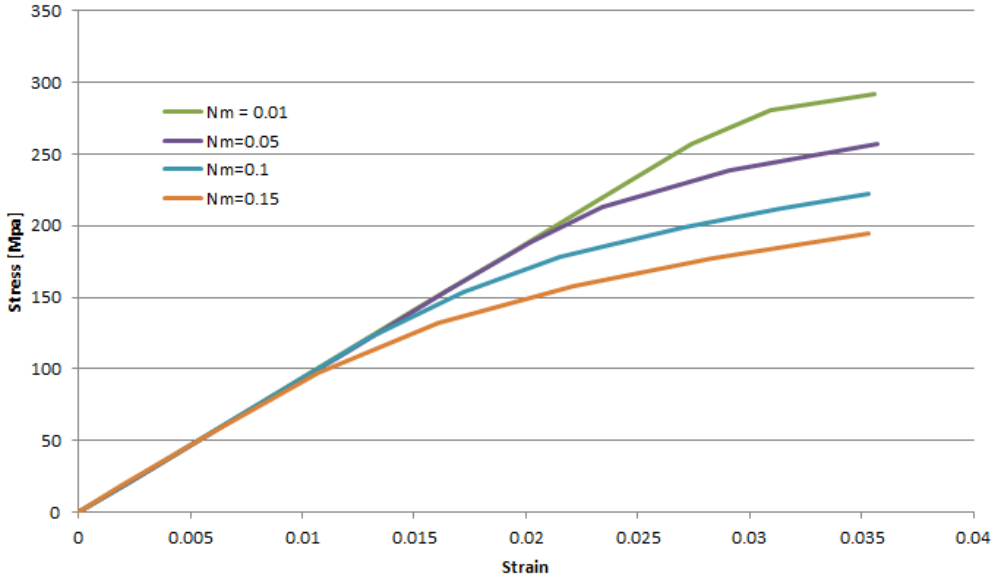

Figure 4.18: Parametric study of N_m

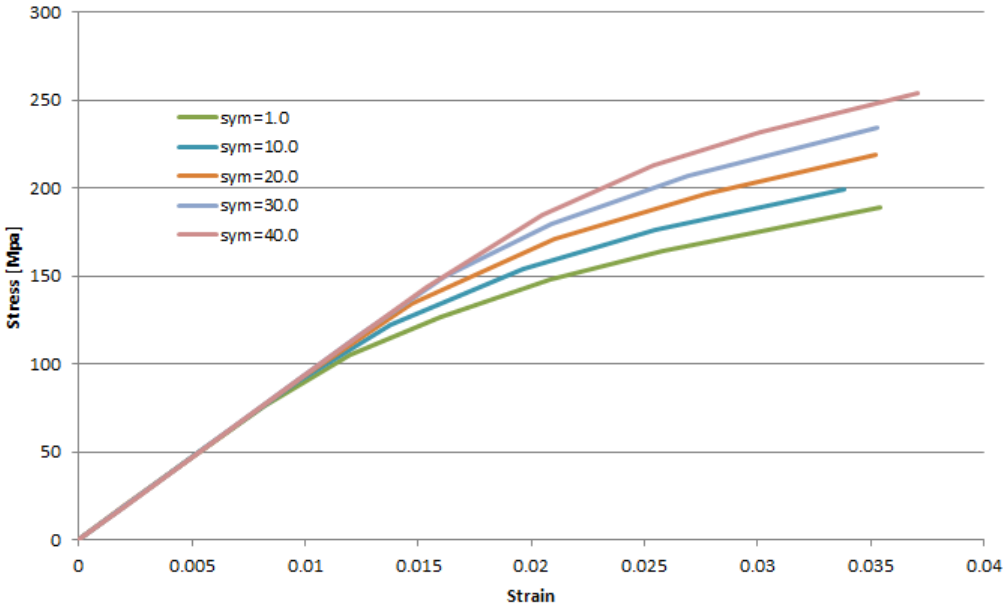

Figure 4.19: Parametric study of σ_{ym}

The Mori-Tanaka parameter modifies how the partioning is performed in the homogenization steps. A Mori-Tanaka term of 1 biases the averaging towards the forwards averaging scheme, as seen in Eq. 3.38. In the forward scheme, more of the material response is dominated by the matrix behaviour, whereas a bias toward the backwards scheme (a lower Mori-Tanaka value) tends the behaviour towards the linear fibre behaviour.

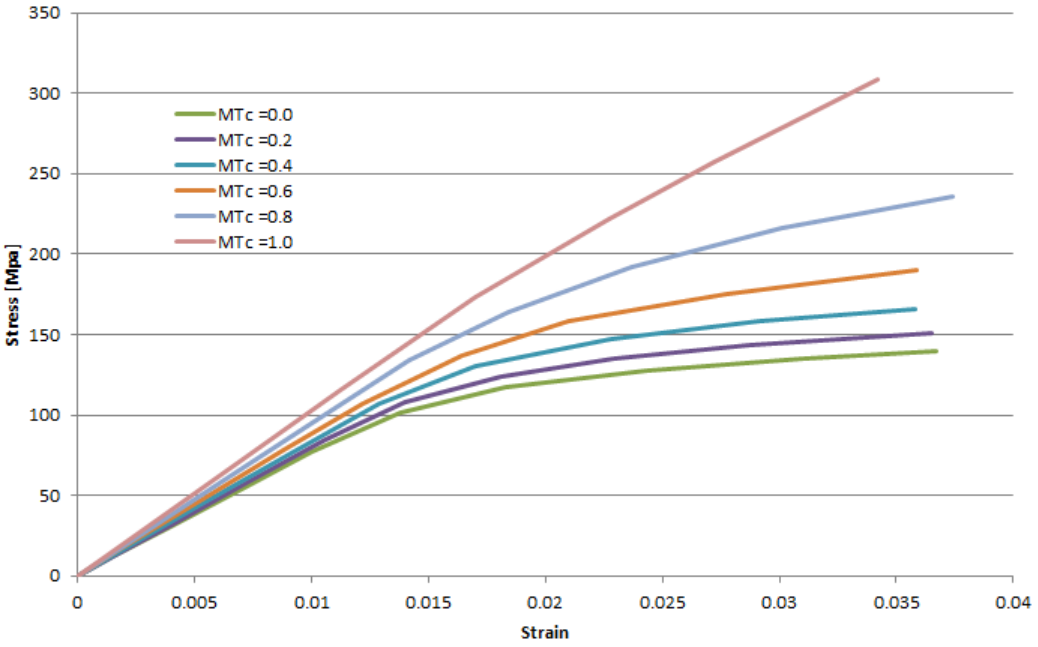

Figure 4.20: Parametric study of MTc

Chapter 5

Conclusion

The framework developed in this thesis is able to accurately simulate the stress-strain response of unidirectional composite materials. A model such as this is used by industrial partners to model the behaviour and failure of a part before it is made for production, saving time and money.

The predicted stress-strain response of a unidirectional material from this model shows good agreement with the experimental results. Both the elastoplastic Sabiston model and the simulation show good agreement with the Hsiao experimental data. A small number of inputs are used in this model, and it primarily contains physically-based parameters.

Elastic and elasto-plastic constitutive models are run to generate predictive stress-strain curves. In the longitudinal and transverse tension, there is very good agreement between the simulated results and the experimental data of an AS4/APC-2 material. However, in both the longitudinal and transverse compression, the simulation deviates from the experimental results, though the effect is more pronounced in the transverse direction.

After incorporating plasticity, the simulation is able to accurately predict the stress-strain results in the longitudinal and transverse tension and compression, as well as shear. This includes failure of the material in each load case for the same AS4/APC-2 material. The longitudinal and transverse compression and shear results are also accurately predicted for an IM6G/3501-6 material as well.

Strain rate experimental data for the AS4/APC-2 material are compared against simulated results. The model is able to predict the rate-dependent behaviour of the material at multiple strain rates.

Through parametric studies, it is possible to know the effect that the pairing parameters and the hardening parameters have on the stress-strain response. Increasing k and l increases the slope of the curve, whereas increasing m can increase or decrease the curve depending on the strain. Increasing the hardening modulus, K_m, increases the magnitude and hardening slope of the curve, whereas increasing N_m decreases the magnitude of the curve. Increasing σ_{ym} increases the yield point of the matrix material, and consequently impacts the yield point of the overall material, and increasing MTc biases the overall response toward the fibrous response.

To conclude, an elasto-visco-plastic constitutive model has been developed for unidirectional composite materials. The predictive capabilities of this model allow the stress-strain curve for a given material to be simulated. This type of model is useful for the automotive and aerospace industry as it allows for a part to be simulated and loaded to failure, instead of manufacturing the part to be physically tested. These simulations can reduce the cost of and time for product development, which ultimately can allow for more composite parts being introduced into working vehicles.

Chapter 6

Future Recommendations

As this model does provide good agreement with experimental data, these recommendations are intended as suggestions to extend the predictive behaviour to a wider variety of applications.

Because glass fibres do display strain-rate dependency, investigating how these effects could be integrated into this model would allow for accurate prediction for both glass and carbon-fibre strain-rates. Further work needs to be done to incorporate these effects.

Although failure of the material has been modelled, damage of the material still impacts the overall behaviour. Failure only shows the point where the material is no longer able to perform its function. In a unidirectional material, this is the overall failure of the material. In a laminate, this would correspond to a failure of a ply, though the overall material would still be capable of carrying load. Before failure, damage is accumulated in the material. In addition to mechanical softening, damage in a composite material could account for some of the reduction in stress shown in a stress-strain curve. Incorporating damage into a material could also allow for simulations involving the generation of cracks or other microscopic failure methods. Having both damage and failure in a model would extend its applicability.

Another recommendation would be to consider giving the user the option of which failure criteria to use. The Chang and Chang criteria is implemented in the current failure model but there are many different failure criteria available in literature. Implementing more than one failure criteria with input flags would allow the user to choose which criteria to use for a given simulation, which would change how conservative a simulated model would be. As well, the Chang and Chang failure criteria is a stress-based criteria. Because the stress-strain curves of the tested materials do not plateau, there is a unique point

on each graph where a strain gives a specific stress. However, for other materials, there could be a plateau on stress. In this case, it would be more advantageous to implement a strain-based criteria, as the stress-based criteria would not be useful.

In addition to mechanical loads that many parts undergo, thermal stresses play a role in loading. For instance, heating of a thermoplastic matrix will change the behaviour of the composite. Therefore, it is recommended that temperature dependence be incorporated into the constitutive behaviour of the model.

References

[1] J. Aboudi. Micromechanical analysis of composites by the method of cells. *Applied Mechanics Reviews*, 42(7):193–221, July 1989.

[2] J. Achenbach and H. Zhu. Effect of interfacial zone on mechanical behavior and failure of fiber-reinforced composites. *Journal of Mechanics and Physics of Solids*, 37(3):381–393, 1989.

[3] D. Adams and S. Tsai. The influence of random filament packing on the transverse stiffness of unidirectional composites. *Journal of Composite Materials*, 3:368–381, July 1969.

[4] V. Azzi and S. Tsai. Anisotropic strength of composites. *Experimental Mechanics*, pages 283–288, 1965.

[5] A. Baker, S. Dutton, and D. Kelly. *Composite Materials for Aircraft Structures*. American Institute of Aeronautics and Astronautics, Inc., 2004.

[6] E. Barbero, G. Abdelal, and A. Caceres. A micromechanics approach for damage modeling of polymer matrix composites. *Composite Structures*, 67:427–436, 2005.

[7] Y. Benveniste. The effective mechanical behavior of composite materials with imperfect contact between the constituents. *Mechanics of Materials*, 4:197–208, 1985.

[8] A. Boresi and R. Schmidt. *Advanced Mechanics of Materials*. John Wiley and Sons, Inc., 2003.

[9] W. Cantwell and J. Morton. The impact resistance of composite materials - a review. *Composites*, 22(5):347–362, September 1991.

[10] E. Car, S. Oller, and E. Onate. A large strain plasticity model for anisotropic materials - composite material application. *International Journal of Plasticity*, 17:1437–1463, 2001.

[11] D. Carlile, D. Leach, D. Moore, and N. Zahlan. Mechanical properties of the carbon fiber/peek composite apc-2/as-4 for structural applications. *Advances in Thermoplastic Matrix Composite Materials*, pages 199–212, 1989.

[12] P. Ponte Castaneda. The effective mechanical properties of nonlinear isotropic composites. *Journal of Mechanics and Physics of Solids*, 39(1):45–71, 1991.

[13] F. Chang and K. Chang. Post-failure analysis of bolted composite joints in tension or shear-out mode failure. *Journal of Composite Materials*, 21:809–833, September 1987.

[14] F. Chang and K. Chang. A progressive damage model for laminated composites containing stress concentrations. *Journal of Composite Materials*, 21:834–855, September 1987.

[15] J. Chen and C. Sun. A plastic potential function suitable for anisotropic fiber composites. *Journal of Composite Materials*, 27(14):1379–1390, 1993.

[16] J. Cheng and W. Binienda. A modified state variable polymer model implementation in ls-dyna. *Earth and Space*, pages 1–8, 2006.

[17] R. Christensen. A critical evaluation for a class of micromechanics models. *Journal of Mechanics and Physics of Solids*, 38(3):379–404, 1990.

[18] Cytec. Apc-2-peek thermoplastic polymer - technical data sheet. 2012. cytec.com.

[19] I. Daniel and T. Liber. Testing fiber composites at high strain rates. *Proceedings of the Second International Conference on Composite Materials*, pages 1003–1018, 1978.

[20] S. Duan, F. Mo, X. Yang, Y. Tao, D. Wu, and Y. Peng. Experimental and numerical investigations of strain rate effects on mechanical properties of lgfrp composite. *Composites Part B*, 88:101–107, 2016.

[21] Stream Engineering. *Digimat User's Manual*. MSC Software Company, 2016.

[22] J. Eshelby. The determination of the elastic field of an ellipsoidal inclusion, and related problems. *Proceedings of the Royal Society of London. Series A, Mathematical, Physical and Engineering Sciences*, 241(1226):376–396, August 1957.

[23] J. Eshelby. The elastic field outside an ellipsoidal inclusion. *Proceedings of the Royal Society of London. Series A, Mathematical, Physical and Engineering Sciences*, 252(1271):561–569, October 1959.

[24] P. Gotsis, C. Chamis, and L. Minnetyan. Prediction of composite laminate fracture: Micromechanics and progressive fracture. *Composites Science and Technology*, 58:1137–1149, 1998.

[25] J. Hallquist. *LS-DYNA Theory Manual*. Livermore Software Technology Corporation, 2006.

[26] J. Harding. Impact damage in composite materials. *Science and Engineering of Composite Materials*, 1(2):41–68, 1989.

[27] L. Hart-Smith. Predictions of a generalized maximum-shear-stress failure criterion for certain fibrous composite laminates. *Composites Science and Technology*, 58:1179–1208, 1998.

[28] L. Hart-Smith. Predictions of the original and truncated maximum-strain failure models for certain fibrous composite laminates. *Composites Science and Technology*, 58:1151–1178, 1998.

[29] Z. Hashin. Analysis of properties of fiber composites with anisotropic constituents. *Journal of Applied Mechanics*, 46:543–550, September 1979.

[30] Z. Hashin. Failure criteria for unidirectional fiber composites. *Journal of Applied Mechanics*, 47:329–334, June 1980.

[31] S. Hayes and D. Adams. Rate sensitive tensile impact properties of fully and partially loaded unidirectional composites. *Journal of Testing and Evaluation*, 10(2):61–68, 1982.

[32] R. Hill. A self-consistent mechanics of composite materials. *Journal of the Mechanics and Physics of Solids*, 13:213–222, 1965.

[33] R. Hill. *The Mathematical Theory of Plasticity*. Clarendon Press, 1971.

[34] M. Hinton and P. Soden. Predicting failure in composite laminates: The background to the exercise. *Composites Science and Technology*, 58:1001–1010, 1998.

[35] O. Hoffman. The brittle strength of orthotropic materials. *Journal of Composite Materials*, 1:200–206, 1967.

[36] H. Hsiao and I. Daniel. Nonlinear elastic behavior of unidirectional composites with fiber waviness under compressive loading. *Journal of Engineering Materials and Technology*, 118:561–570, October 1996.

[37] H. Hsiao and I. Daniel. Strain rate behavior of composite materials. *Composites Part B*, 29B:521–533, 1998.

[38] S. Hsu, T. Vogler, and S. Kyriakides. Inelastic behavior of an as4/peek composite under combined transverse compression and shear. part ii: Modeling. *International Journal of Plasticity*, 15:807–836, 1999.

[39] S. Hsu, T. Vogler, and S. Kyriakides. On the axial propagation of kink bands in fiber composites. part ii: Analysis. *International Journal of Solids and Structures*, 36:575–595, 1999.

[40] J. Hutchinson and H. Jensen. Models of fiber debonding and pullout in brittle composites with friction. *Mechanics of Materials*, 9:139–163, March 1990.

[41] M. Jalalvand, G. Czel, and M. Wisnom. Numerical modelling of the damage modes in ud thin carbon/glass hybrid laminates. *Composites Science and Technology*, 94:39–47, April 2014.

[42] A. Kallimanis and E. Kontou. Tensile strain-rate response of polymeric fiber composites. *Polymer Composites*, pages 572–579, 2005.

[43] M. Karim and M. Hoo Fatt. Rate-dependent constitutive equations for carbon fiber-reinforced epoxy. *Polymer Composites*, pages 513–528, 2005.

[44] A. Kaw. *Mechanics of Composite Materials - 2nd Edition*. Taylor and Francis Group, 2006.

[45] S. King, T. Sabiston, M. Mohammadi, and K. Inal. New phenomenological failure model for composite materials from a homogenized micromechanics approach. *ECCM17 - 17th European Conference on Composite Materials*, June 2016.

[46] V. Kushch, S. Shmegera, and L. Mishnaevsky Jr. Explicit modeling the progressive interface damage in fibrous composite: Analytical vs numerical approach. *Composite Science and Technology*, 71(7):989–997, May 2011.

[47] S. Kyriakides, R. Arseculeratne, E. Perry, and K. Liechti. On the compressive failure of fiber reinforced composites. *International Journal of Solids and Structures*, 32(6/7):689–738, 1995.

[48] U. Lindholm. Some experiments with the split hopkinson pressure bar. *Journal of Mechanics and Physics of Solids*, 12:317–335, 1964.

[49] K. Liu and S. Tsai. A progressive quadratic failure criterion for a laminate. *Composites Science and Technology*, 58:1023–1032, 1998.

[50] P. Liu and J. Zheng. Progressive failure analysis of carbon fiber/epoxy composite laminates using continuum damage mechanics. *Materials Science and Engineering A*, 485:711–717, 2008.

[51] C. Lopes, P. Camanho, Z. Gurdal, and B. Tatting. Progressive failure analysis of tow-placed, variable-stiffness composite panels. *International Journal of Solids and Structures*, 44:8493–8516, 2007.

[52] Livermore Software Technology Corporation (LSTC). Ls-dyna keyword user's manual, volume ii - material models, February 2012.

[53] P. Maimi, P. Camanho, J. Mayugo, and C. Davila. A continuum damage model for composite laminates - part i - constitutive model. *Mechanics of Materials*, 39:897–908, 2007.

[54] T. Mori and K. Tanaka. Average stress in matrix and average elastic energy of materials with misfitting inclusions. *Acta Metallurgica*, 21:571–574, May 1973.

[55] M. Moure, S. Sanchez-Saez, E. Barbero, and E.J. Barbero. Analysis of damage localization in composite laminates using a discrete damage model. *Composites Part B*, 66:224–232, 2014.

[56] S. Murakami. *Continuum Damage Mechanics*. Springer, 2012.

[57] R. Ochola, K. Marcus, G. Nurick, and T. Franz. Mechanical behaviour of glass and carbon fibre reinforced composites at varying strain rates. *Composite Structures*, 63:455–467, 2004.

[58] D. O'Dwyer, N. O'Dowd, and C. McCarthy. Micromechanical investigation of damage processes at composite-adhesive interfaces. *Composite Science and Technology*, 86:61–69, September 2013.

[59] O. Okoli. The effect of strain rate and failure modes on the failure energy of fibre reinforced composites. *Composite Structures*, 54:299–303, 2001.

[60] O. Okoli and A. Abdul-Latif. Failure in composite laminates: Overview of an attempt at prediction. *Composites Part A*, 33(3):315–321, 2002.

[61] O. Okoli and G. Smith. The effect of strain rate and fibre content on the poisson's ratio of glass/epoxy composites. *Composite Structures*, 48:157–161, 2000.

[62] E. Perdahcioglu and H. Geijselaers. Constitutive modeling of two phase materials using the mean field method for homogenization. *International Journal of Material Forming*, 4(2):93–102, 2011.

[63] M.J. Pindera, H. Khatam, A. Drago, and Y. Bansal. Micromechanics of spatially uniform heterogeneous media: A critical review and emerging approaches. *Composites Part B*, 40:349–378, 2009.

[64] A. Puck. *Festigkeitsanalyse von Faser-Matrix-Laminaten*. Hanser Fachbuch, 1996.

[65] J. Qu. Eshelby tensor for an elastic inclusion with slightly weakened interface. *Journal of Applied Mechanics*, 60:1048–1050, 1993.

[66] J. Reis, J. Coelho, A. Monteiro, and H. da Costa Mattos. Tensile behavior of glass/epoxy laminates at varying strain rates and temperatures. *Composites Part B: Engineering*, 43(4):2041–2046, June 2012.

[67] A. Rotem. Prediction of laminate failure with the rotem failure criterion. *Composites Science and Technology*, 58:1083–1094, 1998.

[68] T. Sabiston, M. Mohammadi, M. Cherkaoui, J. Levesque, and K. Inal. Micromechanics based elasto-visco-plastic response of long fibre composites using functionally graded interphases at quasi-static and moderate strain rates. *Composites Part B*, 100:31–43, 2016.

[69] T. Sabiston, M. Mohammadi, M. Cherkaoui, J. Levesque, and K. Inal. Micromechanics for a long fibre reinforced composite model with a functionally graded interphase. *Composites Part B*, 84:188–199, 2016.

[70] C. Schultheisz and A. Waas. Compressive failure of composites, part i - testing and micromechanical theories. *Progress in Aerospace Sciences*, 32:1–42, 1996.

[71] K. Schweizerhof, K. Weimar, Th. Munz, and Th. Rottner. Crashworthiness analysis with enhanced composite material models in ls-dyna - merits and limits. *LS-DYNA World Conference*, 1998.

[72] R. Sierakowski, G. Nevill, C. Ross, and E. Jones. Dynamic compressive strength and failure of steel reinforced epoxy composites. *Journal of Composite Materials*, 5:362–377, 1971.

[73] P. Soden, M. Hinton, and A. Kaddour. A comparison of the predictive capabilities of current failure theories for composite laminates. *Composites Science and Technology*, 58:1225–1254, 1998.

[74] C. Sun and J. Chen. A simple flow rule for characterizing nonlinear behavior of fibre composites. *Journal of Composite Materials*, 23:1009–1020, October 1989.

[75] C. Sun and J. Chen. A micromechanical model for plastic behavior of fibrous composites. *Composites Science and Technology*, 40:115–129, 1991.

[76] R. Talreja. Assessment of the fundamentals of failure theories for composite materials. *Composites Science and Technology*, 105:190–201, 2014.

[77] H. Tan, Y. Huang, C. Liu, and P. Geubelle. The mori-tanaka method for composite materials with nonlinear interface debonding. *International Journal of Plasticity*, 21:1890–1918, 2005.

[78] T. Tay, H. Ang, and V. Shim. An empirical strain rate-dependent constitutive relationship for glass-fibre reinforced epoxy and pure epoxy. *Composite Structures*, 33:201–210, 1995.

[79] S. Tsai. Structural behavior of composite materials. *NASA Contractor Report*, NASA CR-71, July 1964.

[80] S. Tsai. Strength characteristics of composite materials. *NASA Contractor Report*, NASA CR-224, 1965.

[81] S. Tsai and E. Wu. A general theory of strength for anisotropic materials. *Journal of Composite Materials*, 5:58–80, January 1971.

[82] J. Tzeng and A. Abrahamian. An experimental method for compressive properties of laminated composites at high rates of loading. *Journal of Thermoplastic Composite Materials*, 11:133–143, March 1998.

[83] T. Vogler and S. Kyriakides. Inelastic behavior of an as4/peek composite under combined transverse compression and shear. part i: Experiments. *International Journal of Plasticity*, 15:783–806, 1999.

[84] C. Weeks and C. Sun. Modeling non-linear rate-dependent behavior in fiber-reinforced composites. *Composites Science and Technology*, 58:603–611, 1998.

[85] M. Xie and D. Adams. A plasticity model for unidirectional composite materials and its applications in modeling composites testing. *Composites Science and Technology*, 54:11–21, 1995.

[86] J. Yuan, N. Takeda, and A. Waas. Impact compressive failure of gfrp unidirectional composites. *Design and Manufacturing of Composites - Proceedings of the Second Joint Canada-Japan Workshop on Composites*, pages 81–84, August 1998.